

# 國立交通大學

電機學院光電顯示科技產業研發碩士班

## 碩士論文

具可調變電流畫素電路於非晶矽薄膜電晶體  
主動式矩陣有機發光二極體顯示器之實現

**Implementation of a-Si:H TFT AMOLED Display With  
Adaptive Current Scaling Pixel Circuit**

研究生：楊佳峰

指導教授：謝漢萍 教授

中華民國九十六年一月

具可調變電流畫素電路於非晶矽薄膜電晶體  
主動式矩陣有機發光二極體顯示器之實現

**Implementation of a-Si:H TFT AMOLED Display With  
Adaptive Current Scaling Pixel Circuit**

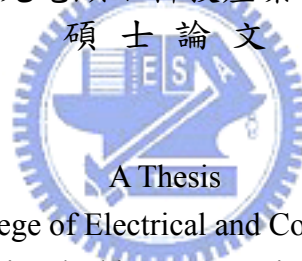
研 究 生：楊佳峰

Student: Chia-Feng Yang

指 導 教 授：謝漢萍

Advisor: Dr. Han-Ping D. Shieh

國立交通大學  
電機學院光電顯示科技產業研發碩士班



Submitted to College of Electrical and Computer Engineering  
National Chiao Tung University  
in partial Fulfillment of the Requirements  
for the Degree of  
Master  
in

Industrial Technology R & D Master Program on  
Photonics and Display Technologies

January 2007

Hsinchu, Taiwan, Republic of China

中華民國九十六年一月


# 具可調變電流畫素電路於非晶矽薄膜電晶體 主動式矩陣有機發光二極體顯示器之實現

學生：楊佳峰

指導教授：謝漢萍

國立交通大學電機學院產業研發碩士班

## 摘 要



主動式有機發光二極體顯示器電流源畫素電路之缺點，在於顯示低灰階畫面時充電時間過長導致驅動資料的錯誤。本論文藉由與傳統電流源及電流鏡畫素電路之電性比較，證實可調變電流畫素電路的確能有效補償 TFT 特性的變化並且縮短充電時間，更進一步設計具可調變電流畫素電路的 AMOLED 面板，解析度為  $50 \times 50$ ，同時並設計所需之驅動電路。在系統整合方面，我們使用 FPGA 產生信號，經過驅動系統提供可調變電流畫素電路所需之電壓或電流控制信號。最後成功點亮 AMOLED 面板，並可呈現出八個灰階，另外其發光的亮度亦符合可調變電流畫素電路之特性，顯示此電路設計的確可以達到有機發光二極體顯示器高解析、大尺寸之需求。

# **Implementation of a-Si:H TFT AMOLED Display With Adaptive Current Scaling Pixel Circuit**

Student: Chia-Feng Yang      Advisor: Dr. Han-Ping D. Shieh

Industrial Technology R & D Master Program of  
Electrical and Computer Engineering College  
National Chiao Tung University

## **ABSTRACT**

The difficulty that current driven pixel circuit of active matrix organic light emitting diode devices encounters lies in long charging time resulted in data programming error while displaying low gray level images. In this thesis, by comparing the adaptive current scaling pixel circuit with conventional current driven pixel circuit and current mirror pixel circuit, the adaptive current scaling pixel circuit is demonstrated to be able to effectively compensate the threshold voltage variation and improve the charging time. Therefore, the adaptive current scaling pixel circuit is designed and applied to AMOLED panel. The OLED devices are deposited on the active area with  $50 \times 50$  pixel array. Moreover, the driving circuits are designed and fabricated. For the integration of system, the driving signals are generated by FPGA. By passing through the driving circuit system, the driving signals are transferred to suitable voltage/current level values for adaptive current scaling pixel circuit. As result, the AMOLED panel is turned on successfully. Such an AMOLED can display 8 gray scales and the experiment results have achieved with the characteristics of adaptive current scaling pixel circuit. These results indicate that the adaptive current scaling pixel circuit can fulfill the requirement of high resolution and large size AMOLED displays.

## 致 謝

回顧兩年的碩士研究生活，這一路走來，要感謝的人很多。在此，謹以此文表達對您們最誠摯的謝意。

首先我要感謝指導教授—謝漢萍老師提供良好的研究環境、充分的學習資源以及廣泛的研究題材，使我在相關領域的研究上能獲益良多。此外更讓我有機會在英語寫作與表達上能加強訓練。同時謝謝黃乙白老師、鄭榮安博士在論文研究與報告上的指導，以及許根玉老師、戴文智博士在口試時提供寶貴的意見，使本論文能更加完備。

在研究所的日子裡，謝謝實驗室學長姐與學弟妹的指導與幫忙。感謝 Vicowa，很懷念跟 V 老、建智、阿龍一起窩在地下室做電路的日子，還有光爾大洪老闆提供許多寶貴的實務經驗，才能讓我能順利完成研究。另外還有許多其他實驗室學長姐以及幫助過我的人，謝謝你們的協助。

再者，我要感謝跟我一起打拼的同學們，子怡、俞文、映頻、淑萍、虹娟、枝福、健富、郡弘、俊文、卓志、明倫，有你們在學業上的討論以及生活上的分享，讓我的研究生生活充滿無限的歡樂與回憶。

最後，謝謝我的女朋友柔賢以及我的父母親、哥哥、大嫂與可愛的小姪子，謝謝你們對我的關愛與包容，也因為有你們默默的陪伴與支持，我才能無後顧之憂的研究與學習並完成學業。再一次獻上我最誠摯的感謝。

# Table of Contents

Abstract (Chinese).....	i
Abstract (English).....	ii
Acknowledgment.....	iii
Table of Contents.....	iv
Figure Captions.....	vii
List of Tables.....	x
<b>Chapter 1 Introduction.....</b>	<b>1</b>
1.1 Thin Film Transistor For Active Matrix Addressing.....	1
1.2 Driving Mode.....	2
1.2.1 Voltage-Driven Pixel Circuit.....	2
1.2.2 Current-Driven Pixel Circuit.....	4
1.3 Motivation and Objective.....	5
1.4 Organization of This Thesis.....	5
<b>Chapter 2 Principle of Adaptive Current Scaling Pixel Circuit.....</b>	<b>7</b>
2.1 Why Current Scaling Function.....	8
2.2 Adaptive Current Scaling Pixel Circuit.....	9
2.2.1 The Operation of Addressing State.....	10
2.2.2 The Operation of Non-Addressing State.....	11
2.3 Summary.....	13
<b>Chapter 3 Fabrication Technologies and Measurement</b>	
<b>Instruments.....</b>	<b>14</b>
3.1 AMOLED Panel Layout.....	14

3.1.1 Single Pixel Layout.....	14
3.1.2 AMOLED Panel Layout.....	16
3.2 a-Si:H TFT Fabrication Process.....	18
3.3 Organic Light Emitting Diode Fabrication Process.....	20
3.4 Design of External Driving Circuit System.....	21
3.4.1 VHDL Coding and FPGA.....	21
3.4.2 Operational Amplifier Circuit.....	22
3.4.3 Constant Current Source Circuit.....	24
3.4.4 Switching Array Circuit of Scan Signal.....	25
3.5 Integration of driving circuit system.....	30
3.6 Measurement System.....	33
3.6.1 Electrical Properties Analysis System.....	33
3.6.2 Chroma Meter.....	34
<b>Chapter 4 Experimental Results and Discussion.....</b>	<b>35</b>
4.1 Electrical Characteristic of Current Scaling.....	35
4.2 Comparison of Electrical Characteristics.....	37
4.3 Reliability.....	41
4.3.1 BTS for TFT Device.....	41
4.3.2 BTS for Adaptive Current Scaling Pixel Circuit.....	42
4.4 Optical Characteristics of AMOLED Panel.....	44
4.4.1 Luminance Uniformity.....	44
4.4.2 Gray Level.....	45
4.4.3 Display Image.....	47
4.5 Summary.....	48
<b>Chapter 5 Conclusion and Future Work.....</b>	<b>49</b>

5.1 Conclusion.....49

5.2 Future Work.....50

**Reference.....52**





## Figure Captions

Fig. 1-1.	Conventional voltage-driven pixel circuit for AMOLED display.....	3
Fig. 1-2.	Comparison of luminance uniformity of (a) voltage programming and (b) current programming.....	3
Fig. 1-3.	Schematic diagram of conventional current-driven pixel circuit for AMOLED display.....	4
Fig. 2-1.	Schematic diagram of conventional current-mirror pixel circuit.....	7
Fig. 2-2.	Schematic diagram of adaptive current scaling pixel circuit for AMOLED display.....	10
Fig. 2-3.	The equivalent circuit diagram of the addressing state.....	11
Fig. 2-4.	The equivalent circuit diagram of the non-addressing state.....	12
Fig. 3-1.	(a) Adaptive current scaling pixel circuit and (b) a photograph of the fabricated single pixel circuit.....	15
Fig. 3-2.	The AMOLED panel consists of signal lines, active area, ground and $V_{DD}$ .....	17
Fig. 3-3.	The active area layout of AMOLED panel.....	17
Fig. 3-4.	Flow chart for inversed-staggered back-channel-etch a-Si:H TFT.....	19
Fig. 3-5.	Schematic and molecular structures of bottom-emission OLED.....	20
Fig. 3-6.	Thermal coater system for OLED fabrication.....	21
Fig. 3-7.	The FPGA simulate board.....	22
Fig. 3-8.	The operational amplifier circuit.....	23
Fig. 3-9.	The layout and application of operation amplifier IC LM 324.....	23
Fig. 3-10.	Fig. 3-10. The constant current source circuit.....	24
Fig. 3-11.	The application of adjustable current source IC LM 334 for constant current source circuit.....	25

Fig. 3-12. Schematic of non-symmetrical voltage circuit.....	26
Fig. 3-13. The switching array circuit of scanning signal.....	26
Fig. 3-14. The clipping circuit.....	27
Fig. 3-15. The clipping circuit with a bypass capacitor.....	27
Fig. 3-16. Non-inverse switching circuit from Vcc to ground.....	28
Fig. 3-17. Inverse switching circuit from Vcc to ground.....	29
Fig. 3-18. Another type of inverse switching circuit from Vcc to ground.....	29
Fig. 3-19. Non-inverse switching circuit from Vcc to -Vss.....	30
Fig. 3-20. Schematic of driving circuit system of AMOLED.....	31
Fig. 3-21. Integration of driving circuit system of AMOLED.....	32
Fig. 3-22. (a) The fixture for AMOLED panel driving test and (b) $\pm 30$ V power supply for $V_{DD}$ .....	32
Fig. 3-23. Electrical property analysis system with Agilent 4156A semiconductor analyzer, 41501B pulse generator, and probe station.....	34
Fig. 3-24. Chroma meter CS-200.....	34
Fig. 4-1. $R_{SCALE}$ as a function of $I_{DATA}$ among measurement and simulation results of adaptive current scaling pixel circuit shown in Fig. 2-2. ....	36
Fig. 4-2. Comparison of $I_{OLED\_ON}$ versus $I_{DATA}$ among conventional current-driven, current-mirror, and adaptive current scaling pixels.....	38
Fig. 4-3. Comparison of $I_{OLED\_OFF}$ versus $I_{DATA}$ among conventional current-driven, current-mirror, and adaptive current scaling pixels.....	39
Fig. 4-4. Comparison of $I_{AVG}$ versus $I_{DATA}$ among conventional current-driven, current-mirror, and adaptive current scaling pixels.....	41
Fig. 4-5. The $\Delta V_{TH}$ as function of stress time at $V_{Gate} = 30$ V, $I_{Drain} = 5$ $\mu$ A in the single TFT device.....	42
Fig. 4-6. Comparison of $\Delta I_{OLED\_OFF}$ as a function of stress time among conventional	

	current-driven pixel circuit and adaptive current scaling pixel circuit.....	43
Fig. 4-7.	VESA FPDM standard, “Sampled Uniformity & Color of White Measurement”, requires the LMD to be positioned in five (or optionally nine) positions perpendicular to the screen surface.....	45
Fig. 4-8.	The lighting of AMOLED and the Non-uniformity is <15%.....	45
Fig. 4-9.	The measurement of gray level.....	46
Fig. 4-10.	$I_{AVG}$ and luminance versus $I_{DATA}$ .....	46
Fig. 4-11.	(a) The image we plan display and (b) the real image on panel.....	47



# List of Tables

Table 3-1. The functions of devices and signal lines on single pixel.....15

Table 3-2. The parameters and signals on single pixel.....16

Table 4-1. The parameters of devices for adaptive current scaling pixel circuit.....36

Table 4-2. The parameters used in the condition of measurement.....36

Table 4-3. The parameters of fabricated device for adaptive current scaling pixel circuit.....37

Table 4-4. The specifications of AMOLED panel.....48



# Chapter 1

## *Introduction*

---

Organic light-emitting displays (OLEDs) have great potential to replace liquid crystal displays (LCDs) due to its merits such as high brightness, high contrast ratio, light weight, thin structure, short response time and low-power consumption [1-5]. Owing to the different properties of OLED from LC, the conventional driving methods for LCD may be inapplicable for OLEDs. In this chapter, the overview of the driving methods for OLEDs will be discussed and the objective of this thesis will be resolved accordingly.

### **1.1 Thin Film Transistor For Active Matrix Addressing**

Initially LCD and OLED were driven by passive matrix (PM) addressing mode to achieve maximum performance. Although the PM addressing mode is acceptable, it limits the display size and resolution because the duration of pulsed signal decreases when increasing the display resolution and gray level. Therefore, PM addressing has been replaced by active matrix (AM) addressing for mass information content and large area flat panel displays (FPDs). In AM addressing scheme, field-effect transistors (FETs), such as thin-film transistors (TFTs) are widely adopted since TFTs can be easily fabricated for large size substrate by either amorphous or polycrystalline silicon technologies.

In the OLEDs, low temperature poly-silicon (LTPS) TFTs utilized as a backplane are commonly adopted in AMOLED development because LTPS TFTs can provide much higher current due to its higher mobility than that of hydrogenated

amorphous-silicon (a-Si:H) TFTs. However, the poly-Si in LTPS TFT is crystallized by excimer laser annealing (ELA), where the uniformity control is difficult. Consequently, the crystallization of poly-Si probably varied, thus affecting the threshold voltage, field-effect mobility and sub-threshold. Thus, the uniformity of TFT will be deteriorated to result in non-uniform brightness from pixel to pixel [6]. Besides, complex fabrication process and high cost are also considered for display industries to develop LTPS TFT as well.

Compared to LTPS TFT, using a-Si:H TFTs as the backplane to realize AMOLED needs fewer manufacturing costs and less equipment investment because the a-Si:H can be deposited by using chemical vapor deposition (CVD) without extra process steps. The uniformity of brightness throughout the whole display is satisfactory [7-8]. Therefore, a-Si:H TFTs is more suitable than LTPS TFTs for large size OLEDs.



## 1.2 Driving Modes

The active matrix pixel circuits can be classified into two categories based on the type of input data. The first one is the voltage-driven pixel circuit and the other is current-driven pixel circuit.

### 1.2.1 Voltage-Driven Pixel Circuit

TFT-based electric circuit is the mainstream of LCD, and exhibits good performance. Hence, it is reasonable to implement the same structure, two-TFT voltage-driven circuit, in OLED panel, as shown in Fig. 1-1 [2]. The gate of switching TFT ( $T_1$ ) is connected to  $V_{SCAN}$  line, and the  $V_{DATA}$  driver provides data to the source of  $T_1$  in each pixel circuit. As soon as the  $V_{DATA}$  was written to the pixel, the  $V_{SCAN}$  was switched to low voltage level and the voltage was stored in  $C_{ST}$ . However, the

two-TFTs circuit in OLED panel causes serious problems: threshold voltage ( $V_{TH}$ ) and mobility ( $\mu_{FE}$ ) variations due to the process- and aging-induced the variation of the TFT characteristics. Increasing  $V_{TH}$  and decreasing  $\mu_{FE}$  decrease OLED driving current for the same input data voltage leading to the non-uniformity in brightness of the whole display area shown in Fig. 1-2(a) [9]. Hence, the compensating circuits should be inserted to keep a constant current passing through the OLED.

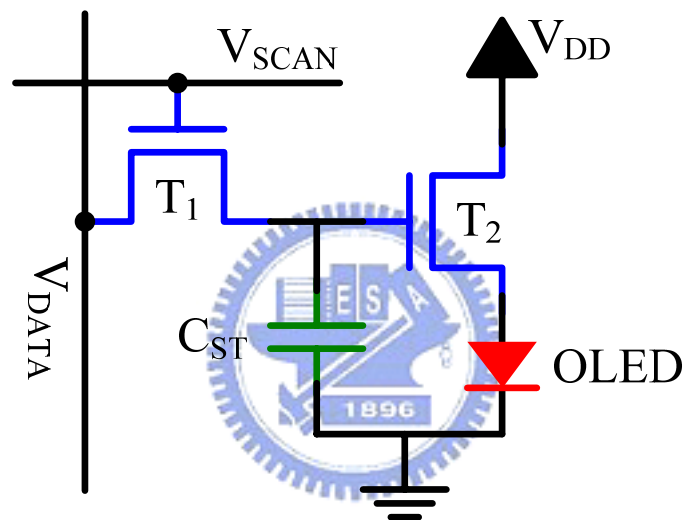


Fig. 1-1. Conventional voltage-driven pixel circuit for AMOLED display.

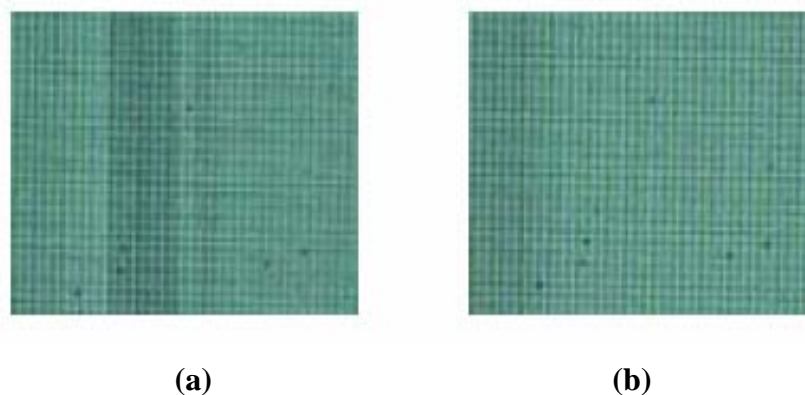


Fig. 1-2. Comparison of luminance uniformity of (a) voltage programming and (b) current programming.

## 1.2.2 Current-Driven Pixel Circuit

Current driving schemes with four-TFT a-Si AMOLED pixel circuit and three control lines shown in Fig. 1-3 was proposed by He et al. [10-11]. A current programmed pixel circuit with self-adjusted voltage source not only provides a continuous excitation to OLED, but also compensates  $V_{TH}$  to improve the brightness uniformity as shown in Fig. 1-2(b). However, a large timing delay is observed at a low programming data current inasmuch as the interaction between the high OLED efficiency and charging of a large interconnected parasitic capacitance. For example, a current of 70 nA is sufficient to achieve luminance of 100 cd/m<sup>2</sup> when the current efficiency of OLED is 20 cd/A or higher, but charging the interconnected parasitic capacitance of about 10 pF to the sufficient voltage level needs more than 150  $\mu$ s. This time period is much longer than the typical frame time (30  $\mu$ s) for a display with VGA (640\*RGB\*80) resolution operated at 60 Hz. As result, the current driving method causes serious data programming error.

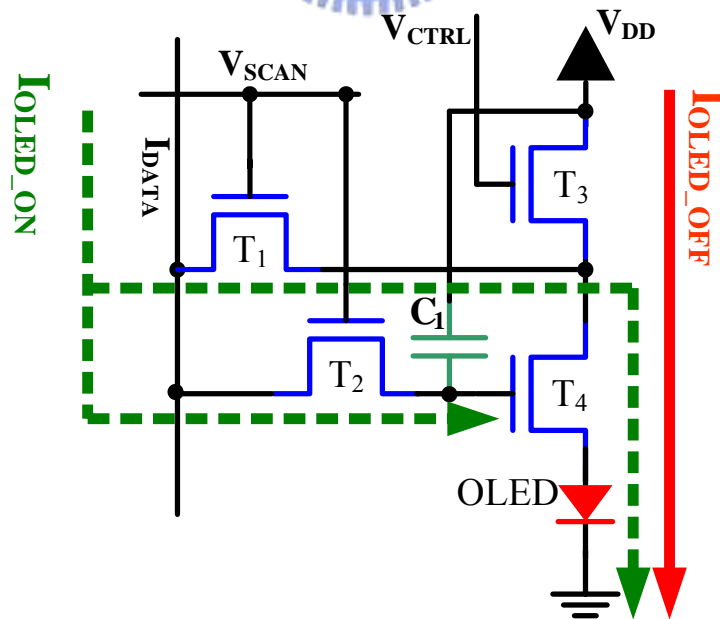


Fig. 1-3. Schematic diagram of conventional current-driven pixel circuit for AMOLED display.



### 1.3 Motivation and Objective

Since the OLED is a current driven device, the pixel circuit needs not only to ensure the matching of current during addressing and non-addressing state, but also to compensate the variations in OLED and TFT characteristics, i.e. threshold voltage variations, aging effects, and etc.

Although a-Si:H TFT technology can reduce manufacturing cost, equipment investment and possess TFT uniformity, poor carrier mobility and larger threshold voltage shift are the main challenges. To resolve these problems, various techniques have been proposed in both voltage and current driven pixel circuits [12-16] using a-Si:H TFTs. In these cases, the current-driven scheme can effectively achieve uniform brightness so that it is suitable for high resolution and large size AMOLED displays. However, in the current-driven mode, low programming data current will induce serious data programming error for high resolution and large size displays.

Therefore, an adjustable current scaling pixel circuit for the a-Si:H TFT was proposed by Y. C. Lin et al. [17] and demonstrated to improve programming time delay. In this thesis, an AMOLED panel with  $50 \times 50$  pixel array based on adaptive current scaling pixel circuit had been implemented and driven by external driving circuit system.

### 1.4 Organization of This Thesis

This thesis is organized and divided into 5 chapters. The principles and the features of adaptive current scaling pixel circuit will be presented in Chapter 2. In Chapter 3, the layout of AMOLED panel, inversed-staggered back-channel-etch a-Si:H TFT and OLED fabrication process will be introduced, respectively. Following are the design and integration of external driving circuit system. Besides, the

measurement equipments used to evaluate electrical properties of adaptive current scaling pixel circuit and visual performance of OLED device with active matrix are illustrated. The experimental results and discussion will be stated in chapter 4. The conclusions of the dissertation and the future works are given in Chapter 5.



# Chapter 2

## *Principle of Adaptive Current Scaling Pixel Circuit*

### *Circuit*

---

Due to the technical challenge for the current-driven pixel circuit for AMOLED displays, the current-mirror type based on current-driven pixel circuit with current scaling function [18-19] that rudimentarily solves programming time delay by using high programming data current to display low gray level images as shown in Fig. 2-1. However, to achieve a large current scaling ratio, the TFT geometric sizes are necessary enlarged, which results in low aperture ratio. Hence, a modified current-driven pixel circuit based on a-Si:H TFT technology with current scaling function which can enhance the data programming speed was proposed and demonstrated. The operation of this pixel circuit and the method of current scaled down will be presented in details as well.

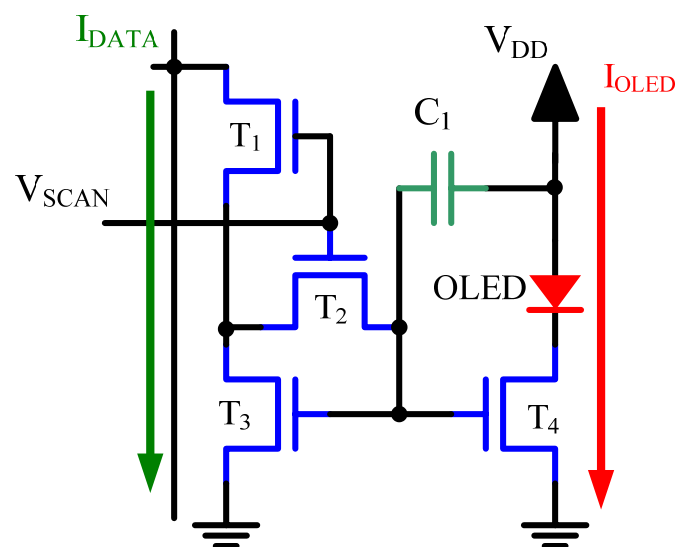


Fig. 2-1. Schematic diagram of conventional current-mirror pixel circuit.

## 2.1 Why Current Scaling Function

The main issue of current-driven pixel circuit in applications for matrix array in pixels display is the long resistance-capacitance (RC) delay, which is proportional to the size and resolution of display panel. A large RC delay will cause cross-talk, flicker effects, and even more serious data programming error due to the insufficient pixel charging across the large display area.

The total programming time ( $T_{PROG}$ ) [20] is defined as the sum of the RC delay time of scan line ( $T_{RC-SCAN}$ ) and data programming time of data line ( $T_{DATA}$ ) written in the following equation:

$$T_{PROG} = T_{RC-SCAN} + T_{DATA}, \quad (2-1)$$

where  $T_{RC-SCAN}$  and  $T_{DATA}$  can be estimated by the following equation:

$$T_{RC-SCAN} = (N_H R_{PIXEL})(N_H C_{PIXEL}) = \frac{R_{\square} C_{\square} H^2}{Z} + N_H C_{OV} R_{\square} H, \quad (2-2)$$

where  $R_{PIXEL}$ ,  $C_{PIXEL}$ ,  $H$ ,  $N_H$ ,  $C_{\square}$ ,  $R_{\square}$ ,  $Z$  and  $C_{OV}$  denote the pixel resistance of bus line, pixel capacitance of bus line, panel width, horizontal resolution, capacitance per meter square, sheet resistance, pixel pitch to bus line width ratio, and TFT gate-to-drain/source overlap capacitance.

$$T_{DATA} = \frac{V_{DATA} (C_{DATA} + C_{ST})}{I_{DATA}}, \quad (2-3)$$

where  $I_{DATA}$ ,  $C_{DATA}$ ,  $C_{ST}$ , and  $V_{DATA}$  denote the programming data current, data line capacitance, storage capacitance and the voltage of  $C_{ST}$ . Due to the  $C_{ST}$  was much smaller than  $C_{DATA}$ , it could be neglected to simplify the calculation. Hence,  $T_{DATA}$  was rewritten as:

$$T_{DATA} \cong \frac{V_{DATA} \cdot N_V \cdot C_{\square}}{R_{SCALE} \cdot J_{OLED} \cdot Z^2}, \quad (2-4)$$

$$R_{SCALE} = \frac{I_{DATA}}{I_{OLED}}, \quad (2-5)$$

$$J_{OLED} = \frac{C_n C_E \pi L}{C_V \eta}, \quad (2-6)$$

where  $N_V$ ,  $R_{SCALE}$  and  $J_{OLED}$  denote the vertical resolution of display, current scaling ratio and the current density of OLED device.  $I_{OLED}$  is the OLED driving current.  $C_n$ ,  $C_E$ , and  $C_V$  depend on the refractive index and the emission spectrum of the OLED material.  $L$  is the OLED luminance and  $\eta$  is device quantum efficiency. Based on Eqs. 2-1 to 2-6, the total programming time can be effectively shortened by large  $R_{SCALE}$  in the condition of the same materials, panel size and resolution. Hence, the combination of current-driven pixel circuit and current scaling function is expected to be widely adopted by the applications in high resolution and large size AMOLED display.

## 2.2 Adaptive Current Scaling Pixel Circuit

The adaptive current scaling circuit consists of a driving TFT ( $T_3$ ), three switching TFTs ( $T_1$ ,  $T_2$ , and  $T_4$ ) and two storage capacitors ( $C_1$  and  $C_2$ ), connected between a scan line and ground with a cascaded structure, as shown in Fig. 2-2. The operation of the circuit is controlled by the ground and four external terminals:  $V_{SCAN}$ ,  $V_{CTRL}$ ,  $I_{DATA}$ , and  $V_{DD}$ . The signals of  $V_{SCAN}$ ,  $V_{CTRL}$ , and  $I_{DATA}$  are supplied by external drivers while the cathode of OLED is connected to the ground. The operation of this pixel circuit is divided into two states: addressing and non-addressing states which are described as follows.

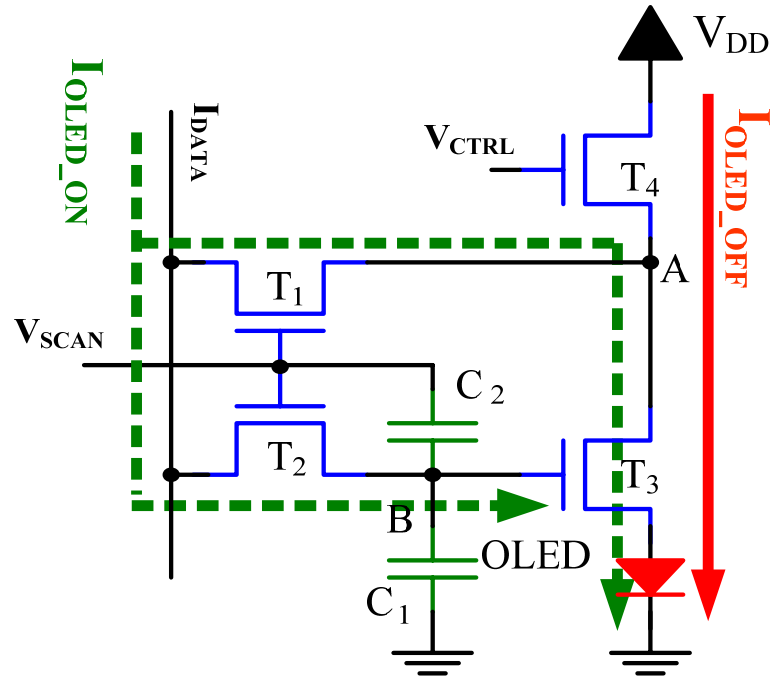


Fig. 2-2. Schematic diagram of adaptive current scaling pixel circuit for AMOLED display.



### 2.2.1 The Operation of Addressing State

During the period of the addressing state,  $T_1$  and  $T_2$  are turned on by  $V_{SCAN}$  and  $T_4$  is turned off by  $V_{CTRL}$ . After that,  $I_{DATA}$  passes through  $T_1$  and  $T_3$  to the OLED device, while a small portion of  $I_{DATA}$  also passes through  $T_2$  to node B. Then, the drain voltage of  $T_3$  (node A) and node B are determined. The equivalent circuit diagram of the addressing state is shown in Fig. 2-3, where  $T_1$  and  $T_2$  are modeled by the turn-on resistance  $R_{T1}$  and  $R_{T2}$ , respectively. Since the  $R_{T1}$  is almost equal to  $R_{T2}$ , node A and node B show the same potential, and  $T_3$  operates in the saturation region, accordingly. Meanwhile, the current passing through the OLED device in the addressing state,  $I_{OLED\_ON}$ , is equal to  $I_{DATA}$ , which also determines the voltages of node A and B. If the variation of threshold voltage of  $T_3$  is smaller than the amplitude of  $V_{SCAN}$ , the gate voltage of  $T_3$ ,  $V_{B-ON}$ , can be adjusted accordingly to ensure constant  $I_{DATA}$  in the addressing state. In other words,  $V_{B-ON}$  is self-adjustable to maintain the

same stable value of  $I_{DATA}$  regardless of threshold voltage variation resulted from the a-Si:H TFT process.

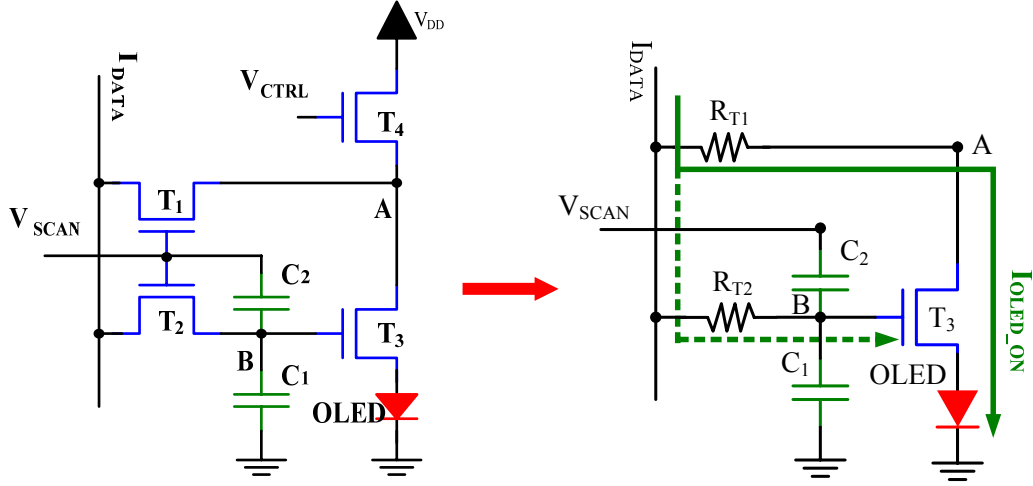


Fig. 2-3. The equivalent circuit diagram of the addressing state.

### 2.2.2 The Operation of Non-Addressing State

During the transition from addressing state to non-addressing state,  $V_{SCAN}$  changes from high to low and then turns off  $T_1$  and  $T_2$ . At the same time,  $T_4$  is turned on by  $V_{CTRL}$  and then the drain electrode of  $T_3$  is connected to  $V_{DD}$  to ensure that  $T_3$  is operated in the saturation region. Subsequently, the current  $I_{OLED\_OFF}$  passes through the OLED device via  $T_4$  and  $T_3$ . The equivalent circuit diagram of the non-addressing state is shown in Fig. 2-4, where  $R_{T4}$  represents the turn-on resistance of  $T_4$ . The voltage at node B drops because of the feed-through effect on the cascaded structure of  $C_1$  and  $C_2$ . The dropped voltage is derived from the charged conversation theory and given by Eq. 2-11. The lower gate voltage of  $T_3$  ( $V_{B-OFF}$ ) is kept on  $C_1$  and  $C_2$  to maintain  $T_3$  turned-on during this period.

$$V_{B-OFF} = V_{B-ON} - \Delta V_{SCAN} \frac{(C_2 \parallel C_{OV-T2})}{C_1 + (C_2 \parallel C_{OV-T2})}. \quad (2-11)$$

In Eq. 2-11,  $\Delta V_{SCAN}$  is the voltage difference of  $V_{SCAN}$  between addressing-state and

non-addressing-state, and  $C_{OV-T2}$  is the gate-to-source/drain overlap capacitance of  $T_2$ .

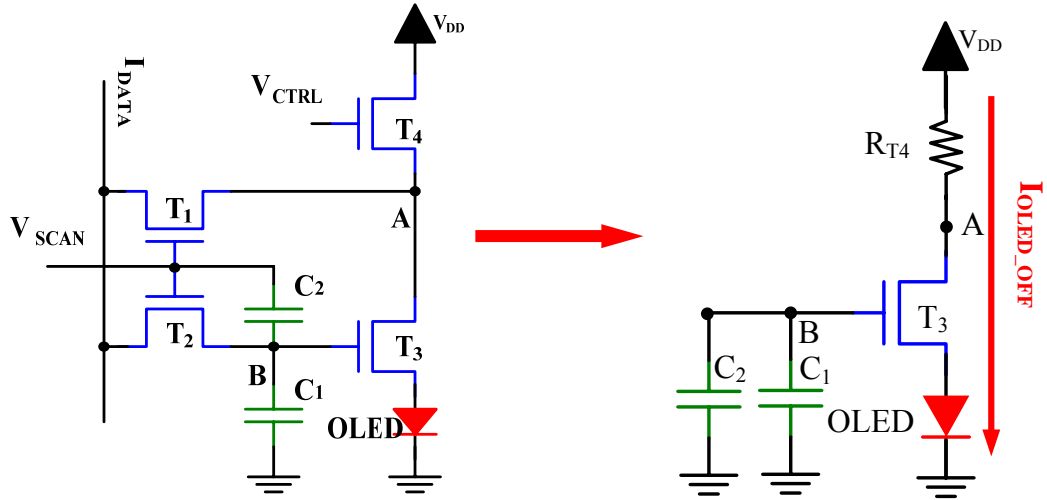


Fig. 2-4. The equivalent circuit diagram of the non-addressing state.

Since the gate voltage of  $T_3$  decreases from  $V_{B-ON}$  to  $V_{B-OFF}$ , the driving current ( $I_{OLED\_OFF}$ ) is scaled down, which can be represented by the current scaling ratio,  $R_{SCALE}$ , defined as:

$$R_{SCALE} = \frac{I_{DATA\_ON}}{I_{OLED\_OFF}}. \quad (2-12)$$

The quantity of voltage drop shown in Eq. 2-11 is proportional to  $\Delta V_{SCAN}(C_2 || C_{OV-T2})/[C_1 + (C_2 || C_{OV-T2})]$  and leads to a small  $I_{OLED\_OFF}$ . Namely,  $R_{SCALE}$  is related to the size of  $C_1$ ,  $C_2$ ,  $C_{OV-T2}$  and  $\Delta V_{SCAN}$ . Since the small geometric size is adequate for  $T_2$ , a small  $C_{OV-T2}$  which is connected to the  $C_2$  in parallel can be regarded as a portion of  $C_2$ . Therefore, the adaptive  $R_{SCALE}$  can be achieved by tuning the ratio of the two cascaded capacitors. Consequently, when a very large programming data current  $I_{DATA}$  is used to charge the pixel electrode and to shorten the pixel programming time, a small driving current  $I_{OLED\_OFF}$  can be achieved for



low gray scales at the same time.

### 2.3 Summary

The adaptive current scaling pixel circuit has a distinguished capability to shorten programming time delay, especially in the low gray levels condition. And the current scaling ratio can be achieved by inserting a small storage capacitor to construct a cascaded capacitors configuration instead of increasing the geometric size of TFTs. Therefore, the  $R_{SCALE}$  is adjusted by tuning the ratio of the two cascaded capacitors without sacrificing the pixel aperture ratio. In the following chapter, how the adaptive current scaling pixel circuit can be realized in the AMOLED applications will be demonstrated and discussed.



# Chapter 3

## *Fabrication Technologies and Measurement*

### *Instruments*

---

To implement the AMOLED panel with adaptive current scaling pixel circuit, hence a  $100 \text{ mm} \times 100 \text{ mm}$  substrate with  $50 \times 50$  pixel array was designed and fabricated. Following, the OLED will deposited onto the pixel array to finish the AMOLED fabrication. To turn on the AMOLED, the driving circuit system was designed and fabricated. It includes operational amplifier circuit, constant current source circuit and circuit array of scan signal. Finally, the driving signal generated by VHDL will control the FPGA to provide the signal to circuit system in order to turn on AMOLED. The layout of AMOLED, fabrication of devices, driving circuit system and measurement instruments will be described in this chapter.

### **3.1 AMOLED Panel Layout**

There is a  $50 \times 50$  pixel array on the AMOLED panel, and some other connected lines of external driving circuit. The detail of the AMOLED panel layout will be described as follows.

#### **3.1.1 Single Pixel Layout**

The single pixel circuit which is shown as Fig. 3-1, consists of a driving TFT, three switching TFTs and two storage capacitors, connected between  $V_{\text{SCAN}}$  and ground with a cascaded structure.  $T_1$ ,  $T_2$  and  $T_4$  are switching TFT,  $T_3$  is driving TFT,  $T_1$  and  $T_2$  are storage capacitor, the functions were shown in Table 3-1. Table 3-2

shows the parameters of devices.

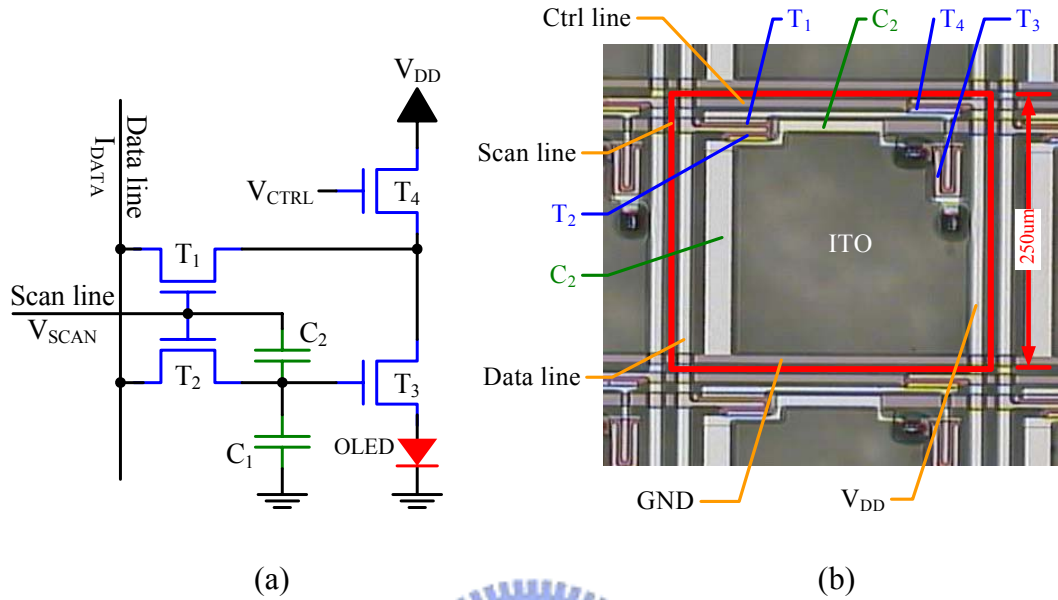


Fig. 3-1. (a) Adaptive current scaling pixel circuit and (b) a photograph of the fabricated single pixel circuit.

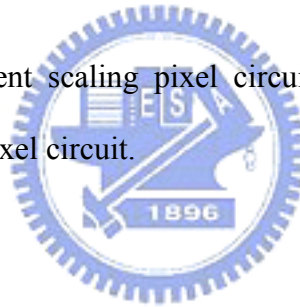


Table 3-1. The functions of devices and signal lines on single pixel.

Device	Function of the device
T <sub>1</sub> , T <sub>2</sub> , T <sub>4</sub>	Switch
T <sub>3</sub>	Driving
C <sub>1</sub> , C <sub>2</sub>	Storing voltages for scaling current

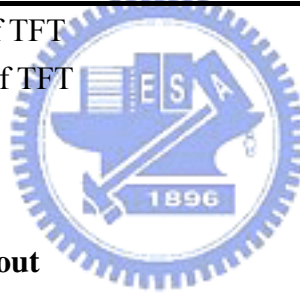
Control signal	Transmitting position
V <sub>SCAN</sub>	Scan line
V <sub>CTRL</sub>	Control line
V <sub>DD</sub>	Direct voltage line
I <sub>DATA</sub>	Data line

Table 3-2. The parameters and signals on single pixel.

<b>Device parameters</b>		
$W^a/L^b$ ( $T_1$ )	( $\mu\text{m}$ )	50/4
W/L ( $T_2$ )	( $\mu\text{m}$ )	30/4
W/L ( $T_3$ )	( $\mu\text{m}$ )	80/4
W/L ( $T_4$ )	( $\mu\text{m}$ )	40/4
$C_1$	(pF)	1.25
$C_2$	(fF)	250
Active Area	( $\mu\text{m}^2$ )	250×250
Aperture Ratio	(%)	52.5
<b>Supplied signals</b>		
$V_{\text{SCAN}}$	(V)	-5~30
$V_{\text{CTRL}}$	(V)	-5~30
$V_{\text{DD}}$	(V)	30
$I_{\text{DATA}}$	( $\mu\text{A}$ )	0.2 ~ 10

<sup>a</sup> channel width of TFT

<sup>b</sup> channel length of TFT



### 3.1.2 AMOLED Panel Layout

The  $50 \times 50$  pixel array AMOLED panel consists of 2500 single pixels as shown in Fig. 3-2. The area of substrate is  $100 \text{ mm} \times 100 \text{ mm}$ , in which scan, ctrl and data lines are included. The active area shown in Fig. 3-3 is located in the central region of the substrate, and the dimension is  $12.5 \text{ mm} \times 12.5 \text{ mm}$ . Otherwise, there are ground and  $V_{\text{DD}}$  on the panel.

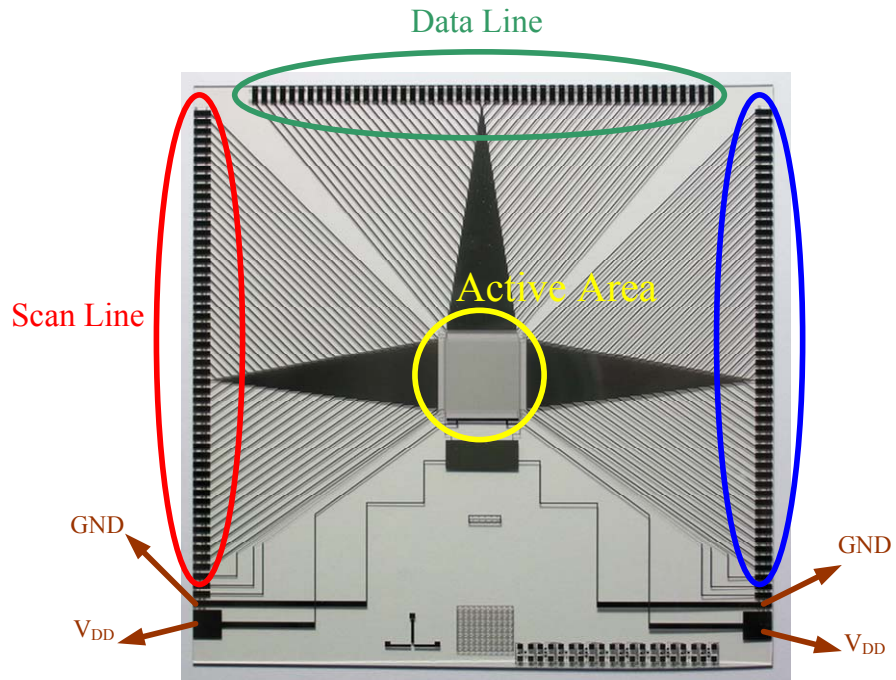


Fig. 3-2. The AMOLED panel consists of signal lines, active area, ground and  $V_{DD}$ .

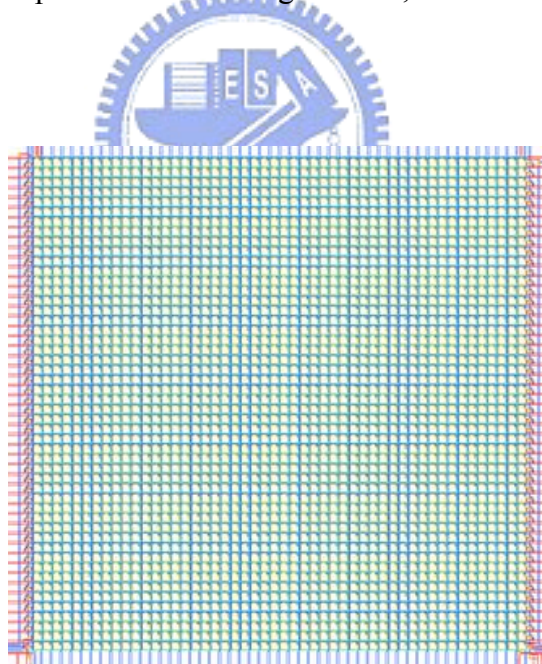


Fig. 3-3. The active area layout of AMOLED panel.

### 3.2 a-Si:H TFT Fabrication Process

The a-Si:H TFT is fabricated by the standard processes of a conventional inversed-staggered back-channel-etch a-Si:H TFT technologies.

Typical process flow for inversed-staggered back-channel-etch a-Si:H TFT [Fig. 3-4]

1. Gate metal deposition on the glass substrate by sputtering method.
2. **Mask #1** : TFT gate electrodes formation, Fig. 3-4(a).
3. Deposition of gate dielectric layer, Fig. 3-4(b).
4. a-Si:H and n<sup>+</sup> a-Si:H layers are sequentially deposited by Plasma Enhanced Chemical Vapor Deposition (PECVD), Fig. 3-4(c).
5. **Mask #2** : active island definition, Fig. 3-4(d).
6. Source/Drain metal deposition by sputtering method.
7. **Mask #3** : Source/Drain electrodes definition, Fig. 3-4(e).
8. n<sup>+</sup> a-Si:H back-channel-etch by the dry etching process, Fig. 3-4(f).
9. Deposition of SiN<sub>x</sub> layer.
10. **Mask #4**: Indium-tin-oxide (ITO) electrode contact hole definition, Fig. 3-4(g).
11. Deposition of ITO layer.
12. **Mask #5**: ITO electrode definition, Fig. 3-4(h).

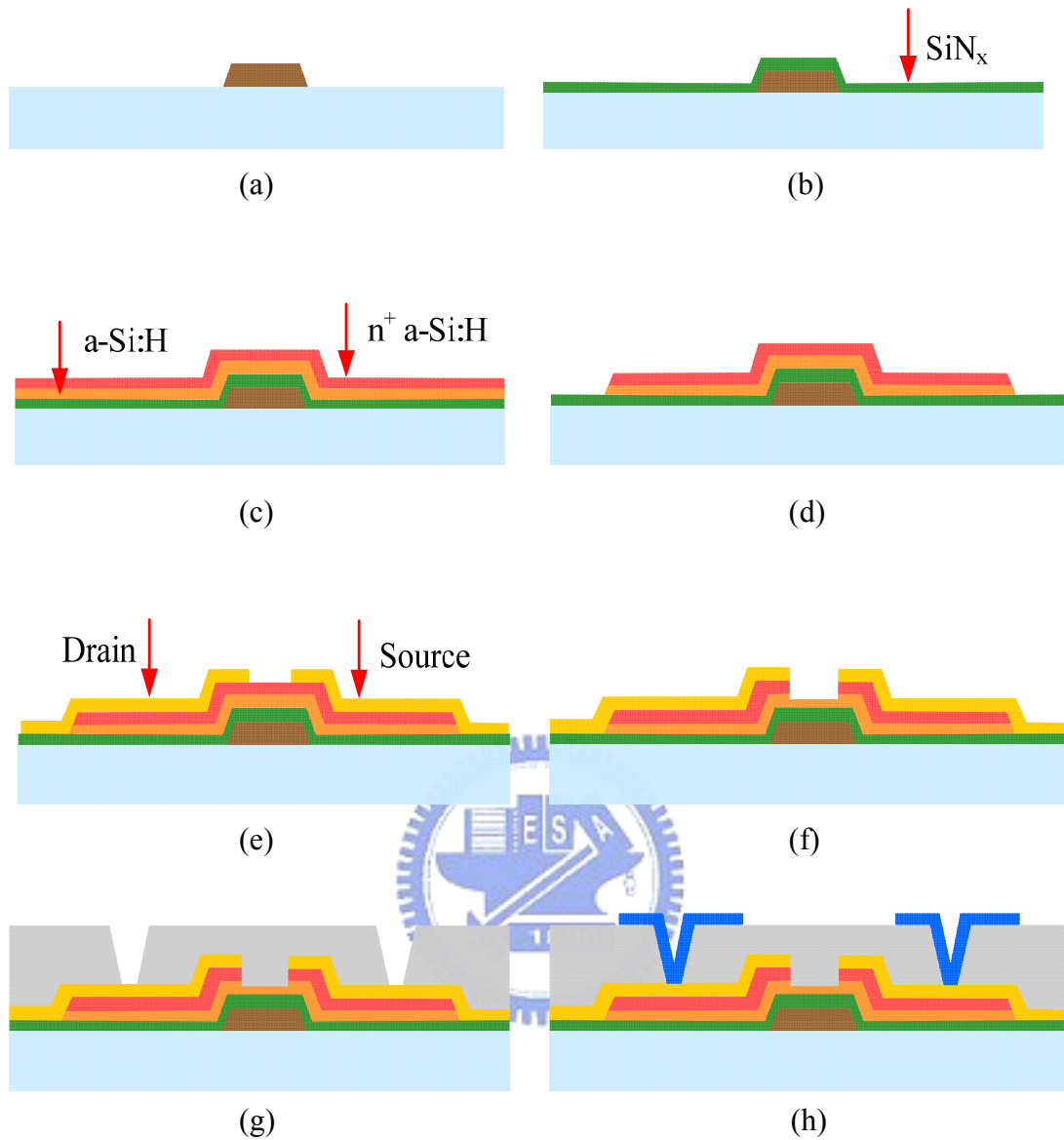


Fig. 3-4. Flow chart for inversed-staggered back-channel-etch a-Si:H TFT.

- (a) Formation of TFT gate electrodes.
- (b) Deposition of gate dielectric layer.
- (c) a-Si:H and n<sup>+</sup> a-Si:H layers deposited by PECVD.
- (d) Active island definition.
- (e) Definition of Source/Drain electrodes.
- (f) n<sup>+</sup> a-Si:H back-channel-etch by the dry etching process.
- (g) Definition of ITO electrode contact holes.
- (h) Definition of ITO electrodes.

### 3.3 Organic Light Emitting Diode Fabrication Process

After the preparation of substrate, an OLED device is deposited onto the TFT backplane to demonstrate the unique performance of the current scaling pixel circuit. The well-known structure of bottom-emission OLED device, ITO / CuPc / NPB / Alq<sub>3</sub> / LiF / Al, is chosen because of its advantages such as high efficiency and stability. All of the device architectures and material structures are shown in Fig. 3-5. These small molecule layers are deposited sequentially by a thermal evaporation process in a chamber to form several parallel thin films which are important for the lifetime of the device as shown in Fig. 3-6.

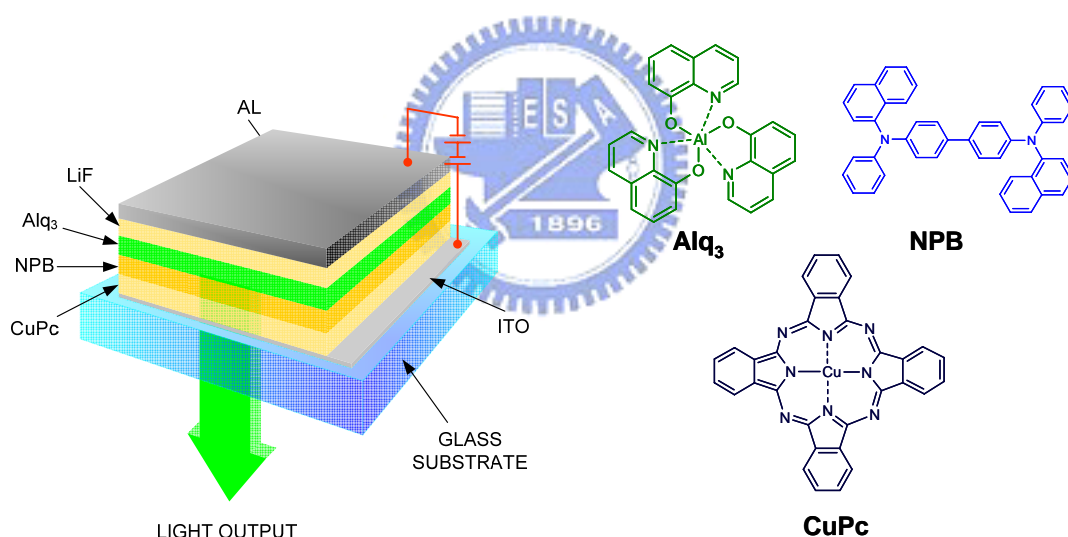


Fig. 3-5. Schematic and molecular structures of bottom-emission OLED.





Fig. 3-6. Thermal coater system for OLED fabrication.

### **3.4 Design of External Driving Circuit System**

This system consists of FPGA simulate board, operational amplifier circuit, constant current source circuit, and circuit array of scan signal. The details of the driving circuit system will be described as follows.

#### **3.4.1 VHDL Coding and FPGA**

The Very-High-Speed Integrated Circuit Hardware Description Language (VHDL) is utilized to program driving signals. Logic Synthesis, Place & Route are verified by Xilinx Integrated Software Environment (ISE™), and Timing Verification is verified by Mentor Modelsim software. The driving signal from FPGA delivers to the driving circuit system which is mentioned above to provide a suitable voltage or current for AMOLED panel.

FPGA is a semiconductor device containing programmable logic components and programmable interconnects. The programmable logic components can be coded to duplicate the functionality of basic logic gates such as AND, OR, XOR, NOT or more complex combinational functions such as decoders or simple math functions. In most FPGAs, these programmable logic components also include memory elements, which may be simple flip-flops or more complete blocks of memories. The FPGA simulate board we used is shown in Fig. 3-7, the chip is Xilinx Spartan XC2S200 PQ208-5, including 200 K gates.

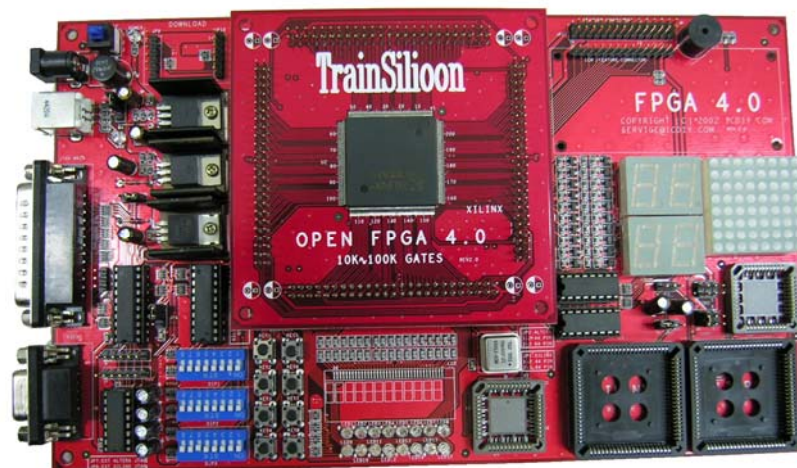


Fig. 3-7. The FPGA simulate board.

### 3.4.2 Operational Amplifier Circuit

Due to the amplitude of signal wave from FPGA is too weak to drive constant current source circuit, the adjustable amplifier circuit shown in Fig. 3-8 is necessary to amplify the amplitude to a proper voltage level. For example, a 3.3 V input signal can be directly amplified to 30 V by operational amplifier IC LM 324 of this circuit.

The layout and application of operational amplifier IC LM 324 are shown in Fig. 3-9. It consists of four independent, high gain, internally frequency compensated

operational amplifiers which were designed specifically to operate from a single power supply over a wide range of voltages. Operation from split power supplies is also workable and the low power supply current drain is independent of the magnitude of the power supply voltage. Application areas include transducer amplifiers, DC gain blocks and all the conventional OP-Amp circuits which now can be more easily implemented in single power supply systems.

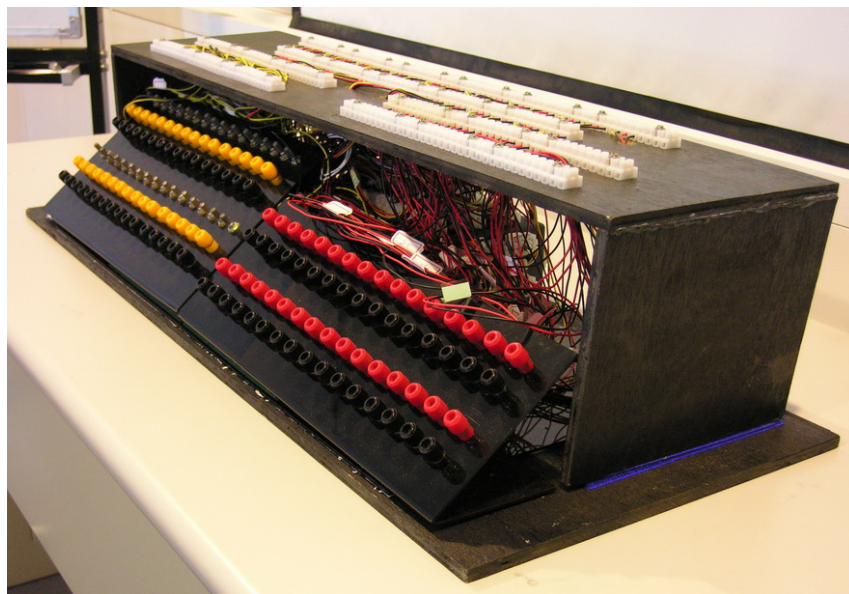


Fig. 3-8. The operational amplifier circuit.

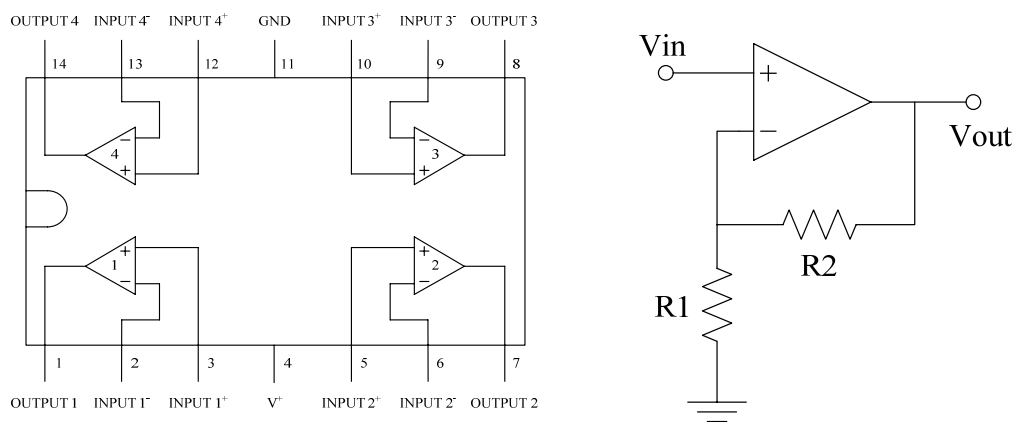


Fig. 3-9. The layout and application of operation amplifier IC LM 324

### 3.4.3 Constant Current Source Circuit

The function of the constant current source circuit shown in Fig. 3-10 provides a suitable data current for AMOLED using adjustable current source IC LM 334 to achieve the resolution of 100 nano-ampere (nA). By introducing the variable resistor, the output current can be adjusted from 1  $\mu$ A to 1 mA.

The LM 334 shown in Fig. 3-11 is a 3-terminal adjustable current source featuring 10,000 : 1 range in operating current, excellent current regulation and a wide dynamic voltage range of 1 V to 40 V. Current is established with one external resistor and no other parts are required. The LM 334 is true floating current sources without separating power supply connections. In addition, reverse applied voltages utmost to 20 V will draw only a few dozen microamperes of current, allowing the devices to act as both a rectifier and current source in AC applications. Applications for the current sources include bias networks, surge protection, low power reference, ramp generation, LED driver, and temperature sensing.



Fig. 3-10. The constant current source circuit.

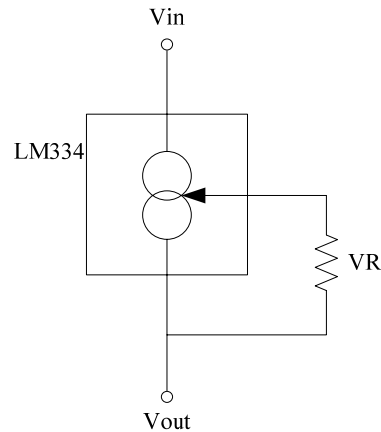


Fig. 3-11. The application of adjustable current source IC LM 334 for constant current source circuit.

### 3.4.4 Switching Array Circuit of Scan Signal

Since the output voltage values of driving signal from FPGA are 0 V & 3.3 V, can not fulfill the requirement of scan and ctrl signal, hence a non-symmetrical voltage circuit which can support -5 V & 30 V is designed, as shown in Fig. 3-12. This circuit includes three part, non-inverse switching circuit from Vcc to ground, inverse switching circuit from Vcc to ground, and non-inverse switching circuit from Vcc to -Vss. As result, a switching array circuit based on this non-symmetrical voltage circuit which can support -5 V & 30 V is implemented and is being shown in Fig. 3-13. The details is described in the following.

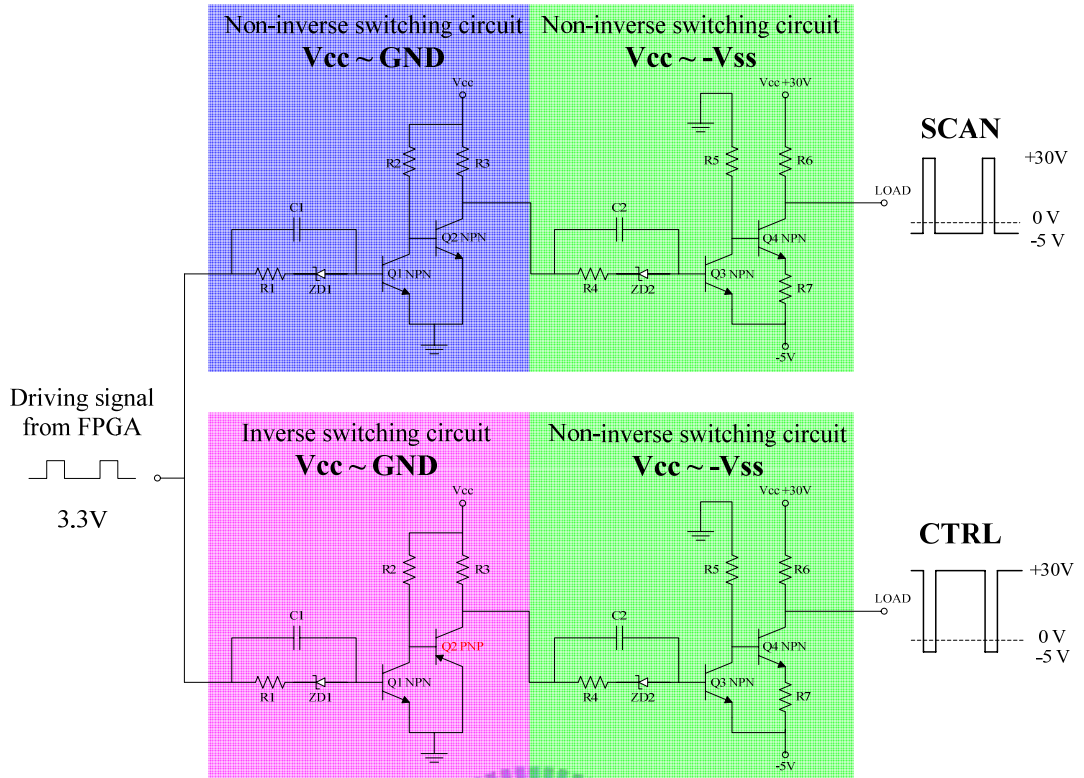


Fig. 3-12 Schematic of non-symmetrical voltage circuit.

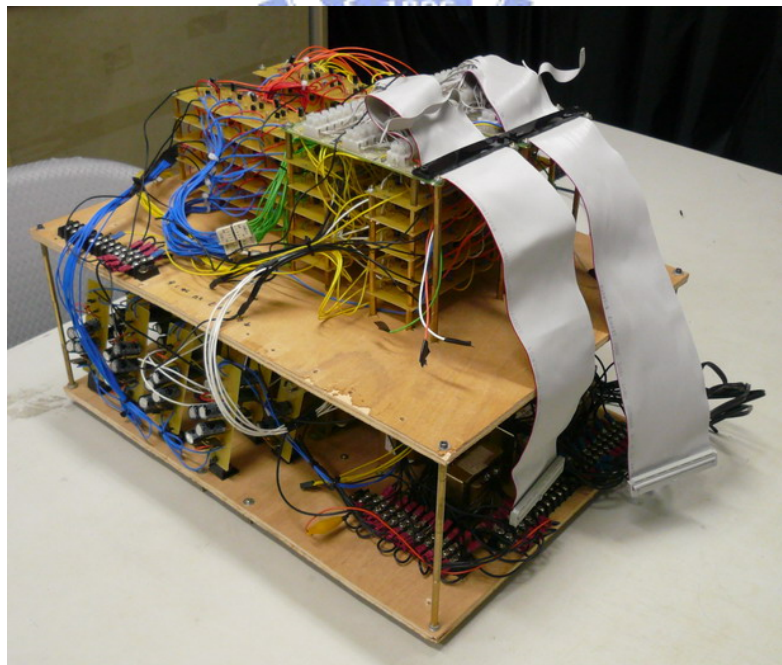


Fig. 3-13 The switching array circuit of scanning signal.

➤ Clipping circuit

A clipping circuit used to control voltage level is shown in Fig. 3-14. An oscillate signal passes through the resistance R1 and Zener diode at voltage  $V_x$ . The input current from  $V_{in}$  will be confined by the resistance R1 to avoid Zener diode been burned-out.  $V_x$  is clipped to the bias voltage  $V_y$  of Zener diode. For example, if there was a Zener diode with bias voltage 3.3 V in clipping circuit, then the input voltage  $V_{in}=5$  V would shift to 3.3 V.



Fig. 3-14. The clipping circuit.

An electrolytic capacitor used to clipping circuit as a bypass capacitor can be applied to high frequency switching circuit as shown in Fig. 3-15. There is a 10  $\mu$ F electrolytic capacitor in array of high frequency switching circuit for AMOLED driving signal. If the frequency of switching circuit larger than 100 MHz, the ceramic capacitor C101 should be replaced by electrolytic capacitor. The functions of clipping circuit are to change voltage level and to keep waveform of  $V_{in}$ .

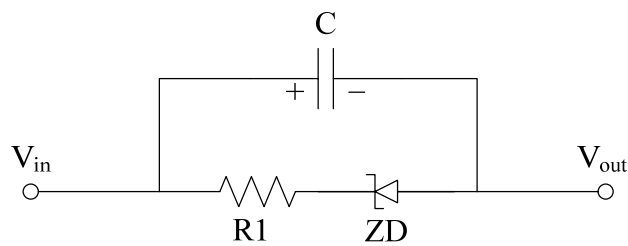


Fig. 3-15. The clipping circuit with a bypass capacitor.

➤ Non-inverse switching circuit from  $V_{cc}$  to ground

Combining a clipping circuit with a Schmitt trigger circuit forms a high frequency switch circuit, as shown in Fig. 3-16. In this circuit, the value of resistance  $R_1$ ,  $R_2$  and  $R_3$  are the same, and transistors  $Q_1$  and  $Q_2$  are also the same, for example 2N2222A or PN9012. The transistors specifics are decided by the frequency of  $V_{in}$  and voltage value of  $V_{cc}$ . The signal of  $V_{in}$  is gained to the same voltage value of  $V_{cc}$  but inversed by the transistor  $Q_1$ . The signal of  $V_{in}$  is kept at the same voltage value of  $V_{cc}$ , but inversed to positive phase by the transistor  $Q_2$  as well. High frequency switching circuit is a usual amplifier for voltage and current. The maximum gain of voltage is equal to  $V_{cc}$ , and the current gain is decided by the current gain coefficient  $h_{FE}$  of transistor.

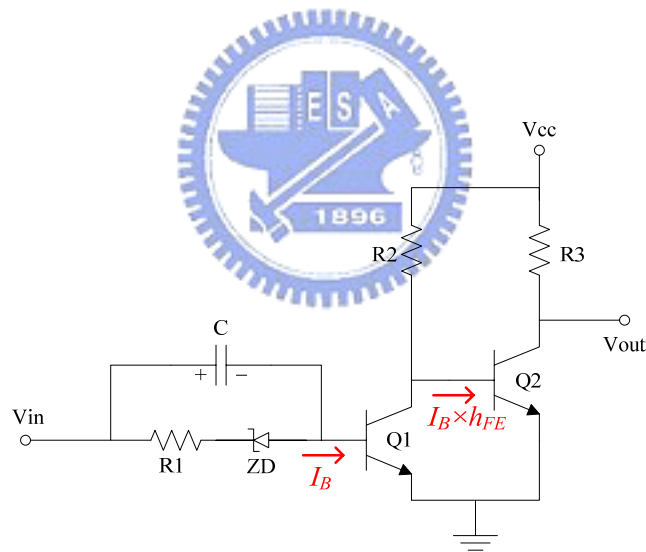


Fig. 3-16. Non-inverse switching circuit from  $V_{cc}$  to ground.

➤ Inverse switching circuit from  $V_{cc}$  to ground

If a PNP transistor instead of  $Q_2$ , we can get an inverse signal switching circuit from  $V_{cc}$  to ground, as shown in Fig. 3-17. The gained  $V_{in}$  signal is equal to that of voltage value of  $V_{cc}$  but inversed by the transistor  $Q_1$ . The signal value of  $V_{in}$  is kept at the same voltage of  $V_{cc}$ , but inversed to positive phase by the transistor  $Q_2$  again.



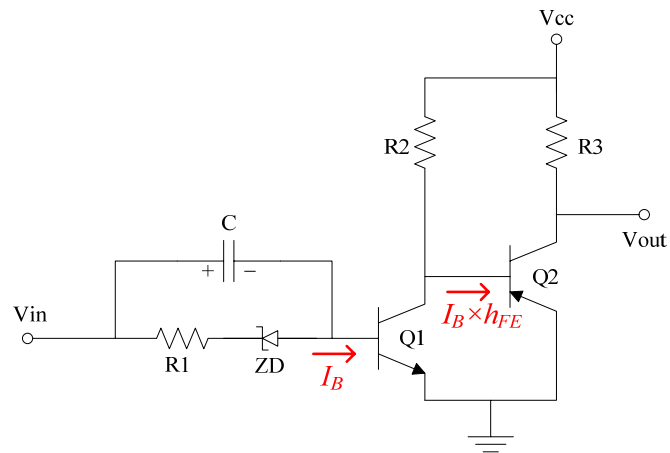


Fig. 3-17. Inverse switching circuit from Vcc to ground.

Non-inverse and inverse switching circuit are basic structure of amplifier IC or comparator IC. Combining inverse buffer CD 4049 with positive phase switching circuit is another inverse switching circuit as shown in Fig. 3-18. There are two limitations of this circuit. One is the cut off voltage while the frequency of  $V_{in}$  is over 500 MHz due to the limitation of voltage rise rate ( $V/\mu s$ ) of inverse buffer CD 4049. The other is that the voltage value of  $V_{in}$  should be larger than the lowest operating voltage 4.5 V of inverse buffer CD 4049.

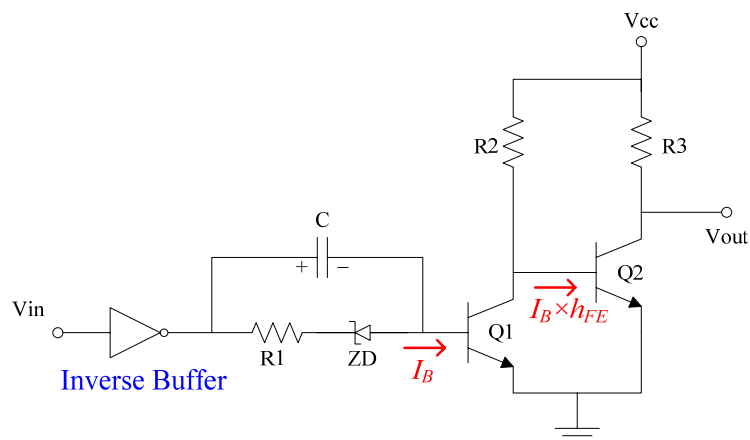


Figure 3-18 Another type of inverse switching circuit from  $V_{cc}$  to ground.

➤ Non-inverse switching circuit from  $V_{cc}$  to  $-V_{ss}$

The clipping circuit added to a Schmitt trigger circuit with alternate power sources will construct a high frequency switching circuit as shown in Fig.3-19. The difference between Fig. 3-16 and Fig. 3-19 located on the schematic diagram. The collector of transistor Q1 of Fig. 3-19 was connected to ground, and the emitter of transistors Q1 and Q2 were connected to  $-V_{ss}$ . The resistance value of R1 should exceed 1 k $\Omega$ , R2 should exceed 5 k $\Omega$ , and the ratio of R3/R4 must exceed 20. The Base-emitter of transistor Q1 will be turned on by the ON signal of  $V_{in}$ , then trigger the collector of transistor Q2 and guide the  $V_{cc}$  to output. The Base-emitter of transistor Q1 will be turned off by the OFF signal of  $V_{in}$ , then interrupt the emitter of transistor Q2 and guide  $-V_{ss}$  to output.

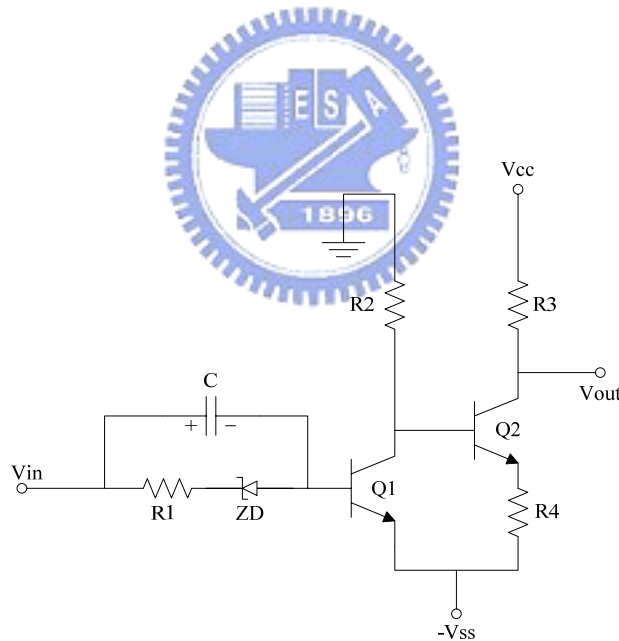


Fig. 3-19 Non-inverse switching circuit from  $V_{cc}$  to  $-V_{ss}$ .

### 3.5 Integration of driving circuit system

To turn on AMOLED, we should integrate the driving circuits and finish the fabrication of AMOLED, as shown in Figs. 3-20 and 3-21. The data signal from FPGA was amplified by the operational amplifier circuit, and generate the

micro-ampere ( $\mu\text{A}$ ) level current for AMOLED by a constant current source circuit. The scan signal from FPGA was amplified and went through to scan and ctrl signals, separately, for AMOLED by passing through circuit array of scan signal. Fig. 3-22(a) shows the fixture for AMOLED panel. The  $V_{DD}$  was provided by external power supply, as shown in Fig. 3-22(b), can provide a  $\pm 30\text{ V}$  voltage value. Fig.3-21 shows the integration of driving circuit system and AMOLED panel.

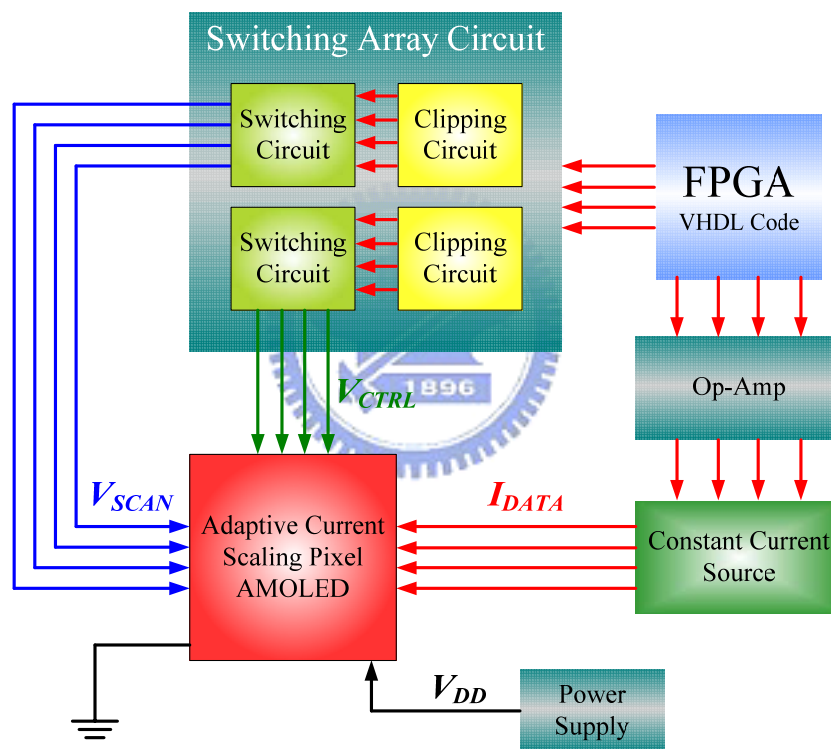


Fig. 3-20. Schematic of driving circuit system of AMOLED.

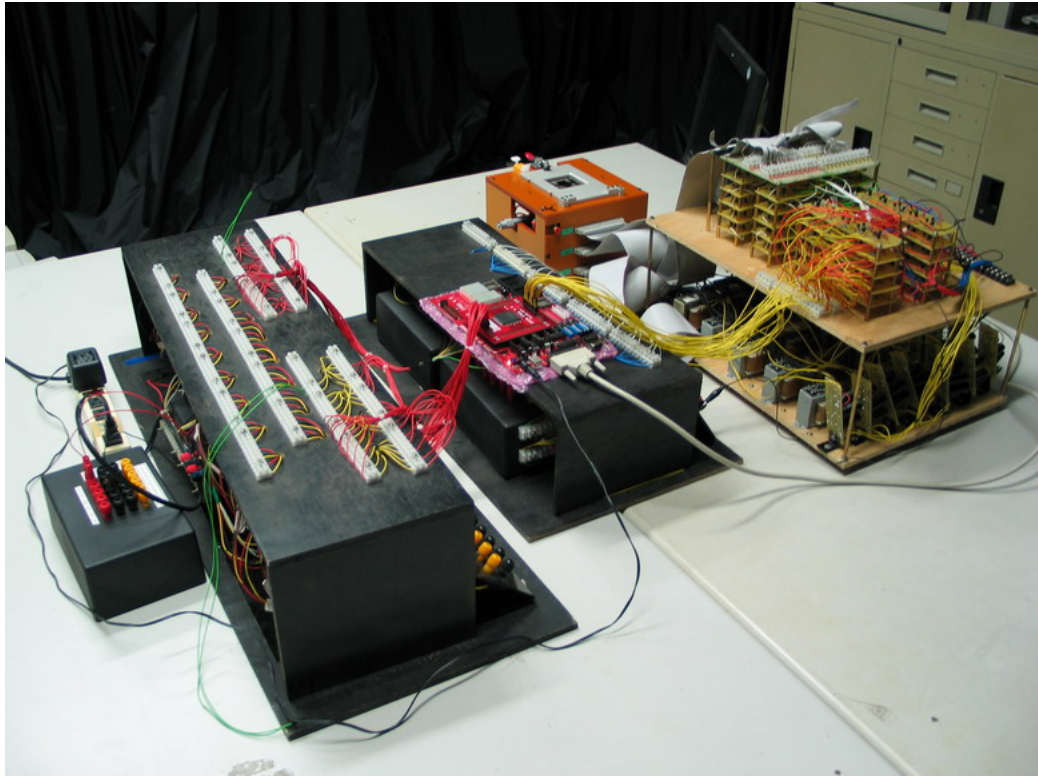
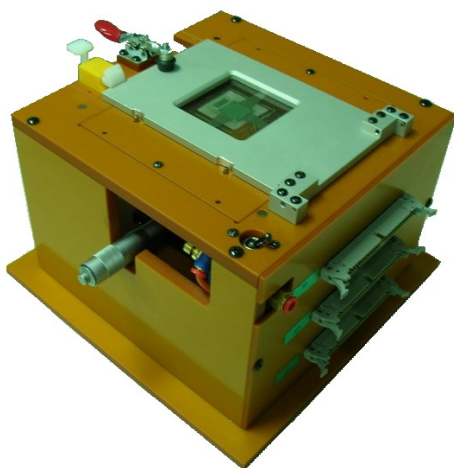


Fig. 3-21. Integration of driving circuit system of AMOLED.



(a)



(b)

Fig. 3-22. (a) The fixture for AMOLED panel driving test and (b)  $\pm 30$  V power supply for  $V_{DD}$ .

## 3.6 Measurement System

After fabricating the AMOLED and driving circuits, the experiments were conducted to confirm that the cell performs in agreement with the original design. The instruments including electrical properties analysis system and chroma meter will be introduced in the following subsections.

### 3.6.1 Electrical Properties Analysis System

The electrical property analysis system mainly consists of Agilent 4156A semiconductor analyzer and 41501B pulse generator, as shown in Fig. 3-23. An Agilent 4156A semiconductor analyzer with a probe station is used to analyze the electrical properties of a circuit such as I-V measurement or bias-temperature-stress (BTS). The ground probe station is furnished with an electrically isolated, water-cooled thermal plate within an optical shielding box. The station can be controlled by Temptronic TPO315A thermal controller between 25 °C and 300 °C. The source measurement units (SMUs) are used to control voltage sources where current flowing through can be measured. The voltage or current sources supplied by Agilent 4156A semiconductor analyzer can be transmitted through SMU to the pixel circuit and the output voltage or current will be detected concomitantly.

In addition, the 41501B pulse generator is employed to create wave function signals which Agilent 4156A semiconductor analyzer cannot provide. Consequently, combining Agilent 4156A semiconductor analyzer with 41501B pulse generator can advance the application for electrical property analysis.

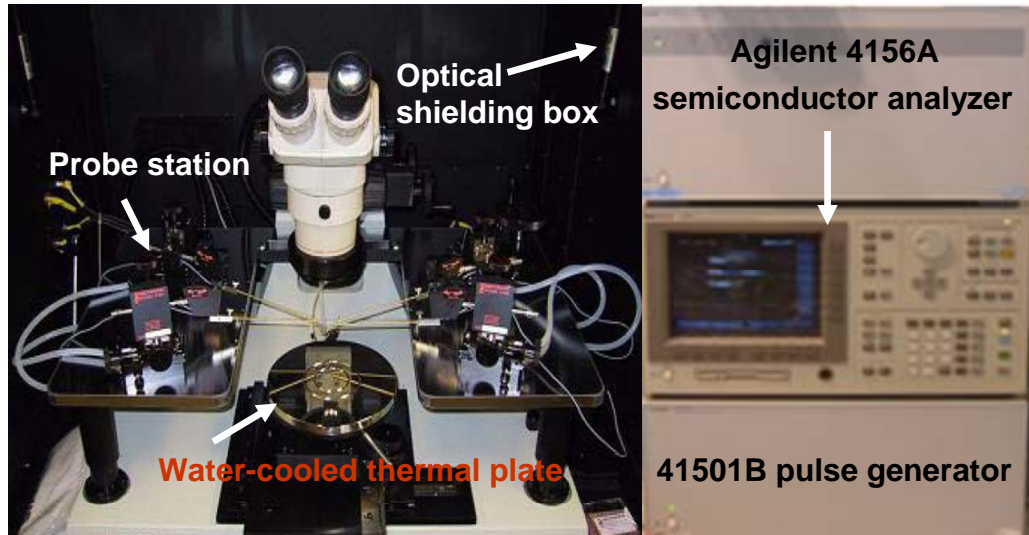


Fig. 3-23. Electrical property analysis system with Agilent 4156A semiconductor analyzer, 41501B pulse generator, and probe station.

### 3.6.2 Chroma Meter

The chroma meter CS-200 shown in Fig. 3-24 can be utilized to measure luminance and chromaticity of various optical devices.

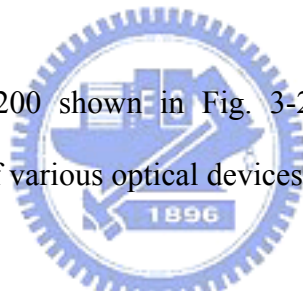


Fig. 3-24. Chroma meter CS-200.

# Chapter 4

## *Experimental Results and Discussion*

---

After fabrication and integration of driving circuit system and AMOLED panel, the experiments were implemented to examine the design. In this chapter, the electrical characteristics and reliability were examined. Besides, OLED materials were deposited onto the a-Si:H TFT panel and been turned on by driving circuits to analyze the visual performance.

### **4.1 Electrical Characteristic of Current Scaling**

The device parameters and measurement conditions of adaptive current scaling pixel circuit are listed in Table 4-1 and Table 4-2. The Agilent 4156A semiconductor analyzer and 41501B pulse generator are used to measure the electrical property as shown in Fig. 3-23. From the measurement results, when the  $R_{SCALE}$  increases from 1.8 to 920 as  $I_{DATA}$  decreases from 10 to 0.2  $\mu A$  shown as the dot line in Fig. 4-1. It is clearly indicated that not only the large  $R_{SCALE}$  at low gray levels but also low  $R_{SCALE}$  at high gray levels are achieved so that the  $R_{SCALE}$  is adjusted by input data current. Hence, the function of the adaptive current scaling pixel circuit on the AMOLED panel is successfully demonstrated.

Table 4-1. The parameters of devices for adaptive current scaling pixel circuit.

Device parameter		
$W^a/L^b$ (T <sub>1</sub> )	( $\mu\text{m}$ )	50/4
W/L (T <sub>2</sub> )	( $\mu\text{m}$ )	30/4
W/L (T <sub>3</sub> )	( $\mu\text{m}$ )	80/4
W/L (T <sub>4</sub> )	( $\mu\text{m}$ )	40/4
C <sub>1</sub>	(pF)	1.25
C <sub>2</sub>	(fF)	250

<sup>a</sup> channel width of TFT

<sup>b</sup> channel length of TFT

Table 4-2. The parameters used in the condition of measurement.

Supplied signals		
V <sub>SCAN</sub>	(V)	0~30
V <sub>CTRL</sub>	(V)	0~30
V <sub>DD</sub>	(V)	30
I <sub>DATA</sub>	( $\mu\text{A}$ )	0.2 ~ 10

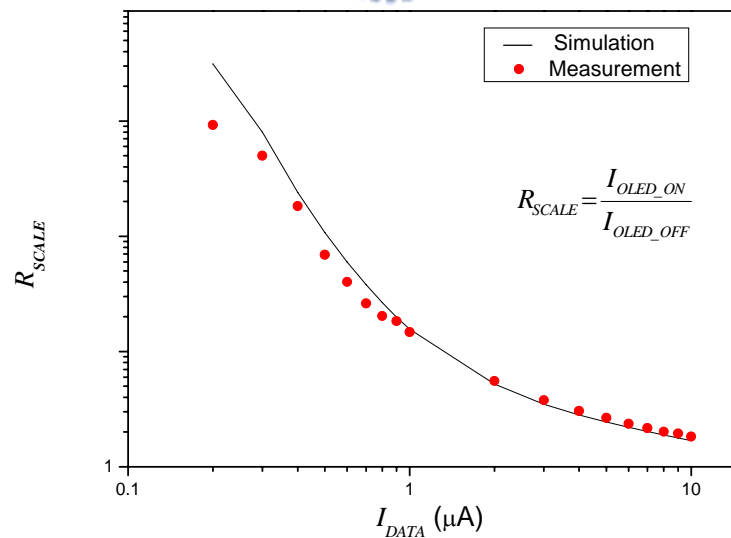


Fig. 4-1.  $R_{SCALE}$  as a function of  $I_{DATA}$  among measurement and simulation results of adaptive current scaling pixel circuit shown in Fig. 2-2.



## 4.2 Comparison of Electrical Characteristics

There are three kinds of testing pixel circuits arranged on the panel in the layout process. Therefore, the electrical characteristics among conventional current-driven (Fig. 1-3), current-mirror (Fig. 2-1) and adaptive current scaling pixel circuits were compared.

The device parameters and measurement conditions of current-driven and current mirror pixel circuit were listed in Table 4-3 and Table 4-2, and adaptive current scaling pixel circuit was in Table 4-1.

Table 4-3. The parameters of fabricated device for adaptive current scaling pixel circuit.

		Current-driven	Current mirror
$W^a/L^b$ ( $T_1$ )	( $\mu\text{m}$ )	100/4	100/4
W/L ( $T_2$ )	( $\mu\text{m}$ )	100/4	100/4
W/L ( $T_3$ )	( $\mu\text{m}$ )	100/4	200/4
W/L ( $T_4$ )	( $\mu\text{m}$ )	50/4	50/4
$C_1$	(pF)	2.5	2.5

<sup>a</sup> channel width of TFT

<sup>b</sup> channel length of TFT

### ➤ Addressing state

For these three kinds of pixel circuits, the driving currents of OLED in the addressing state ( $I_{\text{OLED\_ON}}$ ) were proportional to  $I_{\text{DATA}}$ , as shown in Fig.4-2. In conventional current-driven and adaptive current scaling pixel circuit, the  $I_{\text{OLED\_ON}}$  were equal to  $I_{\text{DATA}}$ . On the other hand, the ratio of  $I_{\text{DATA}}/I_{\text{OLED\_ON}}$  of current mirror pixel circuit was equal to the ratio of  $T_3/T_4$ .

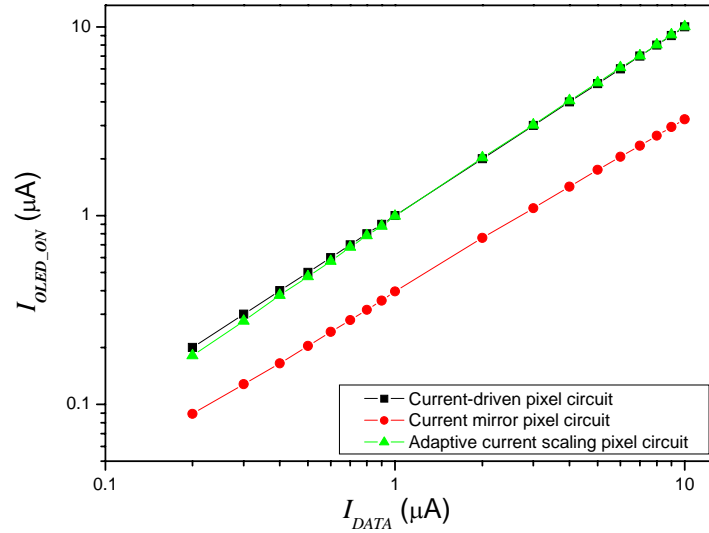


Fig. 4-2. Comparison of  $I_{OLED\_ON}$  versus  $I_{DATA}$  among conventional current-driven, current-mirror, and adaptive current scaling pixels.

➤ Non-Addressing state

The conventional current-driven pixel circuit does not have the capability of current scaled down no matter the geometric size of TFTs changed or not. Therefore, the driving current of OLED in the non-addressing state ( $I_{OLED\_OFF}$ ) of conventional current-driven pixel circuit was still identical to  $I_{DATA}$ . The current mirror pixel circuit was able to scale down  $I_{DATA}$ , but the scale-down ratio was constant in the whole range of  $I_{DATA}$ . However, for the adaptive current scaling function, at  $I_{DATA}$  of 0.2  $\mu A$ , the  $I_{OLED\_OFF}$ , was scaled down to 0.18 nA. On the other hand, at  $I_{DATA}$  of 10  $\mu A$ , the  $I_{OLED\_OFF}$  was scaled down to 4.7  $\mu A$ . It meant that the amount of current drop at lower  $I_{DATA}$  was more than that at higher  $I_{DATA}$  due to the lower  $I_{DATA}$  passed through  $T_3$ , the lower  $V_{B-ON}$  was. Hence, the voltage drop of

$$\Delta V_{SCAN} \cdot \frac{C_2 \parallel C_{OV-T2}}{C_1 + C_2 \parallel C_{OV-T2}}$$

was relatively larger than  $V_{B-ON}$  resulted in the larger current drop of  $I_{DATA}$  so that the larger  $R_{SCALE}$  was obtained at lower gray levels.

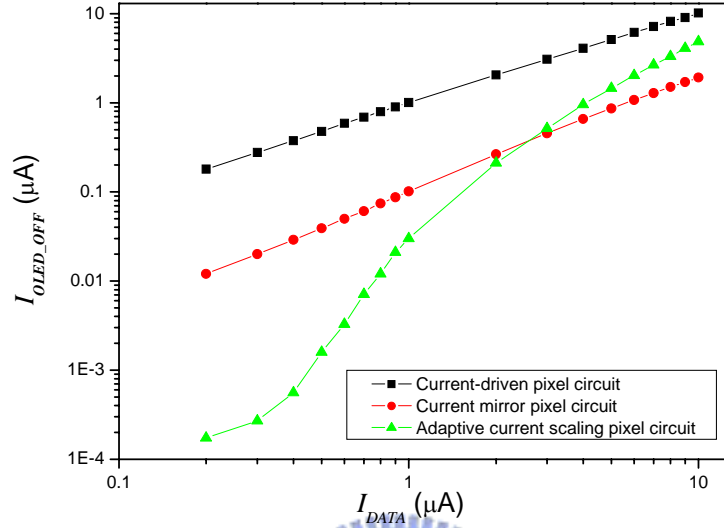


Fig. 4-3. Comparison of  $I_{OLED\_OFF}$  versus  $I_{DATA}$  among conventional current-driven, current-mirror, and adaptive current scaling pixels.

The current scaling function is implemented to reduce the programmed current from addressing state to non-addressing state. Since  $I_{OLED\_ON}$  ( $=I_{DATA}$ ) is larger than  $I_{OLED\_OFF}$  by a factor of  $R_{SCALE}$ , the average OLED current ( $I_{AVG}$ ) [21] for the pixel circuit is

$$I_{AVG} = \frac{I_{OLED\_ON} t_{ON} + I_{OLED\_OFF} t_{OFF}}{t_{ON} + t_{OFF}}, \quad (4-1)$$

where  $t_{ON}$  and  $t_{OFF}$  denote the addressing and non-addressing state periods during the frame time, respectively. Meanwhile, the  $I_{AVG}$  can also be rewritten by Eq. 2-12 as :

$$I_{AVG} = I_{OLED\_OFF} \left[ \frac{R_{SCALE} t_{ON} + t_{OFF}}{t_{ON} + t_{OFF}} \right]. \quad (4-2)$$

Evidently adjusting  $I_{OLED\_OFF}$  and  $R_{SCALE}$  controls  $I_{AVG}$  to achieve different gray levels for display. Subsequently,  $t_{ON}$  of 0.33 ms and  $t_{OFF}$  of 16.33 ms are adopted to calculate the variation of OLED current during a frame time. Moreover,  $t_{ON}$  is much longer than  $t_{OFF}$ , the small  $I_{OLED\_OFF}$  in the non-addressing state can further reduce the  $I_{AVG}$  even if the  $I_{OLED\_ON}$  is large.

To highlight the advantages of adaptive current scaling pixel circuit, the OLED average current ( $I_{AVG}$ ) as a function of data current in the adaptive current scaling pixel circuit as well as the conventional current-driven and current-mirror pixel circuits is shown in Fig. 4-4. In a frame period ( $t_{ON} + t_{OFF}$ ), the  $I_{AVG}$  of the current driven pixel circuit is almost equal to  $I_{DATA}$ , implying no current scaling function existed in the current driven pixel. As to the current mirror pixel, the circuit is able to scale down  $I_{DATA}$ , but the scale-down ratio is constant in the whole range of  $I_{DATA}$ . In addition, in order to achieve higher current scaling function, the TFT size should be larger but the aperture ratio would be reduced. In comparison,  $I_{AVG}$  of the adaptive current scaling pixel circuit achieves the widest range of driving current from 3 nA to 5  $\mu$ A, comparing to current-driven pixel (0.2 to 10  $\mu$ A) and current-mirror pixel (0.01 to 2  $\mu$ A) in the range of  $I_{DATA}$  from 0.2 to 10  $\mu$ A. Hence, at the same programming data current, the lowest gray levels are displayed by the adaptive current scaling pixel circuit. In other words, the adaptive current scaling pixel circuit can be driven by a larger  $I_{DATA}$  to shorten the programming time.

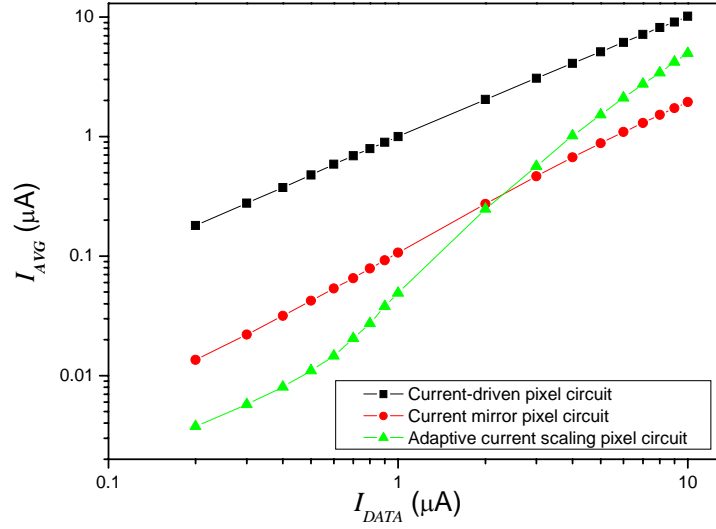


Fig. 4-4. Comparison of  $I_{AVG}$  versus  $I_{DATA}$  among conventional current-driven, current-mirror, and adaptive current scaling pixels.

### 4.3 Reliability

To investigate the effect of threshold voltage ( $V_{TH}$ ) and mobility ( $\mu_{FE}$ ) variation due to device aging or fabrication processes, a bias-temperature-stress (BTS) experiment was performed for TFT device and adaptive current scaling pixel circuit to accelerate the aging process by using the Agilent 4156A with a probe station.

#### 4.3.1 BTS for TFT Device

In the experiment, the channel width and length of TFT device were set to 80 and  $4\mu\text{m}$  while the gate and drain electrodes were supplied 30V and  $5\mu\text{A}$  during the stress time. The threshold voltage deviation,  $\Delta V_{TH}$ , was defined as follows:

$$\Delta V_{TH} = V_{TH\_AS} - V_{TH\_BS}, \quad (4-3)$$

where  $V_{TH\_AS}$  and  $V_{TH\_BS}$  denote the after and before stress of TFT threshold voltage.

The  $\Delta V_{TH}$  of TFT device was a dependence of stress time as shown in Fig. 4-5. At 25

°C,  $\Delta V_{TH}$  varied from 0 to 1.9 V as the stress time increased from 0 to 20000 seconds as shown by the black line in Fig. 4-5. On the other hand, when the temperature was increased to 85 °C, the  $\Delta V_{TH}$  enlarged from 0 to 13 V while stress time increased from 0 to 20000 seconds shown by the red line in Fig. 4-5. The substantial deviation was obtained because hot carrier was trapped at the interface of a-Si and the dielectric layer resulted in the increase of  $\Delta V_{TH}$ .

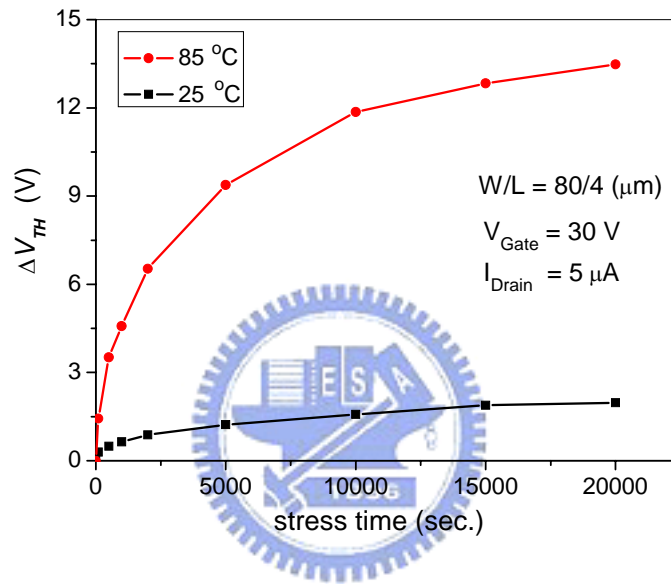


Fig. 4-5. The  $\Delta V_{TH}$  as function of stress time at  $V_{Gate} = 30$  V,  $I_{Drain} = 5$   $\mu$ A in the single TFT device.

### 4.3.2 BTS for Adaptive Current Scaling Pixel Circuit

To research the influence of  $\Delta V_{TH}$  of driving TFT ( $T_3$ ) on pixel circuit performance, a bias-temperature-stress (BTS) experiment was performed to accelerate the aging speed. However, to avoid any OLED-related degradation issues, a diode-connected TFT was connected to source electrode of  $T_3$  instead of the OLED device in the experiment. Based on the Fig. 4-5 results, in the condition of high temperature stress, the aging process was fast. Hence, the operation temperature was set to 85 °C and  $V_{SCAN}$  was kept on 30 V when an  $I_{OLED\_ON}$  of 5  $\mu$ A was applied.

Moreover, the variation of the  $I_{OLED\_OFF}$  ( $\Delta I_{OLED\_OFF}$ ) was defined as:

$$\Delta I_{OLED\_OFF} = \frac{I_{OLED\_OFF}(\Delta V_{TH}) - I_{OLED\_OFF}(\Delta V_{TH} = 0)}{I_{OLED\_OFF}(\Delta V_{TH} = 0)}. \quad (4-4)$$

$\Delta I_{OLED\_OFF}$  as a function of stress time was compared to the conventional current-driven and adaptive current scaling pixel circuits as shown in Fig. 4-6. In the stress time of 1000 seconds, the amount of  $\Delta I_{OLED\_OFF}$  in current-driven pixel circuit was 15 % and 3 % while the  $I_{DATA}$  was 0.5 and 5  $\mu A$ , respectively. Although the  $\Delta I_{OLED\_OFF}$  of the adaptive current scaling pixel circuit was larger than that of current-driven pixel circuit at  $I_{DATA}$  of 0.5  $\mu A$ ,  $\Delta I_{OLED\_OFF}$  of adaptive current scaling pixel circuit could be suppressed to 3.7 % at  $I_{DATA}$  of 5  $\mu A$ . These results indicated that adaptive current scaling pixel circuit was able to compensate for the TFT  $\Delta V_{TH}$  variation to ensure a stable, constant output current level. This would achieve both a good control of the display gray levels and a uniform luminance distribution over the whole AM-OLEDs.

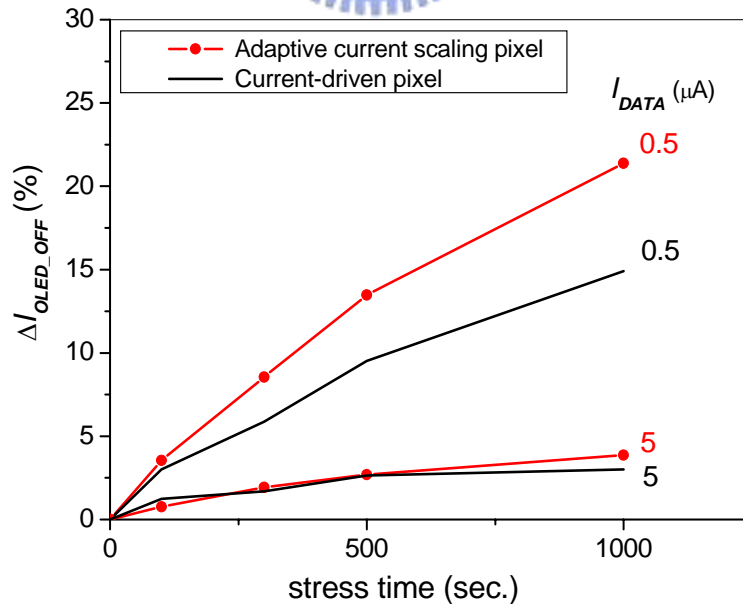


Fig. 4-6. Comparison of  $\Delta I_{OLED\_OFF}$  as a function of stress time among conventional current-driven pixel circuit and adaptive current scaling pixel circuit.

## 4.4 Optical Characteristics AMOLED Panel

### 4.4.1 Luminance Uniformity

The luminance uniformity is measured according to Video Electronics Standards Association (VESA) Flat Panel Display Measurements (FPDM) Standard Version 2.0 (June 1, 2001) [22].

The VESA FPDM luminance uniformity measurement requires that the light-measurement device (LMD) be positioned at five (or optionally nine) locations perpendicular to the screen surface (see Fig. 4-7 for a layout of the VESA uniformity measurement). Measurement locations include the center point plus four (or eight) peripheral points that are always 10 % of screen width from the sides and 10 % of screen height from the top and bottom. As with all VESA FPDM measurements, only the method and reporting format are prescribed; no pass/fail criteria are imposed. A simple “Non-Uniformity” metric is calculated from the five (or nine) measured points as

$$\text{Non-Uniformity} = 100\% \left[ 1 - \left( L_{\min} / L_{\max} \right) \right] \quad (4-5)$$

where  $L_{\min}$  is the minimum and  $L_{\max}$  is the maximum luminance measured. Here, we can see that if  $L_{\min} = L_{\max}$ , the non-uniformity equals zero. If  $L_{\min}$  is 10 % less than the  $L_{\max}$  ( $L_{\min} = 0.9L_{\max}$ ), then the non-uniformity becomes 10 %, which is fairly intuitive. Fig. 4-8 shows the lighting of AMOLED, the non-uniformity is about 14.4 % without concerning dark dots.



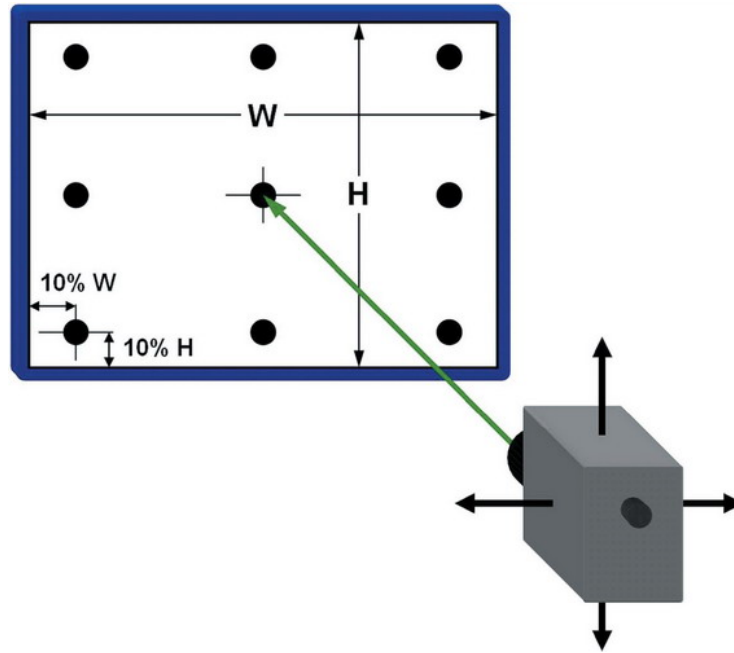


Fig. 4-7 VESA FPDM standard, “Sampled Uniformity & Color of White Measurement”, requires the LMD to be positioned in five (or optionally nine) positions perpendicular to the screen surface.

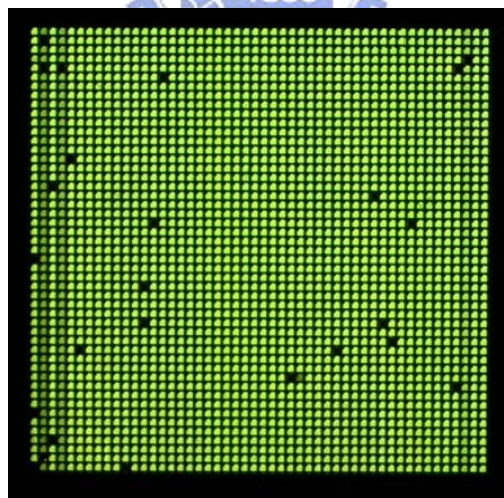


Fig. 4-8 The lighting of AMOLED and the Non-uniformity is <15%

#### 4.4.2 Gray Level

As for measurement of gray level, we select 4 columns with different data current input to display different level. In Fig. 4-9, the varieties of 8 gray scales are

apparent. Owing to the constant current circuit we utilized as power source, the current values of each column are the same. By adjusting the variable resistance of constant current source circuit to get different output currents, afterwards the different gray scales are displayed. On the other hand, the Fig. 4-10 shows the relationship of  $I_{AVG}$  (Fig. 4-4, eq. 4-1), luminance versus input data current ( $I_{DATA}$ ) during the 1  $\mu\text{A}$  ~ 10  $\mu\text{A}$ , and the brightness exhibits the characteristics of current scaling apparently.

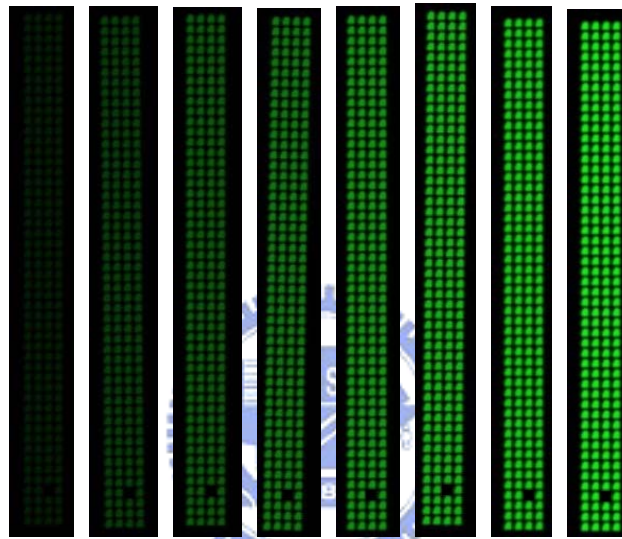


Fig. 4-9 The measurement of gray level.

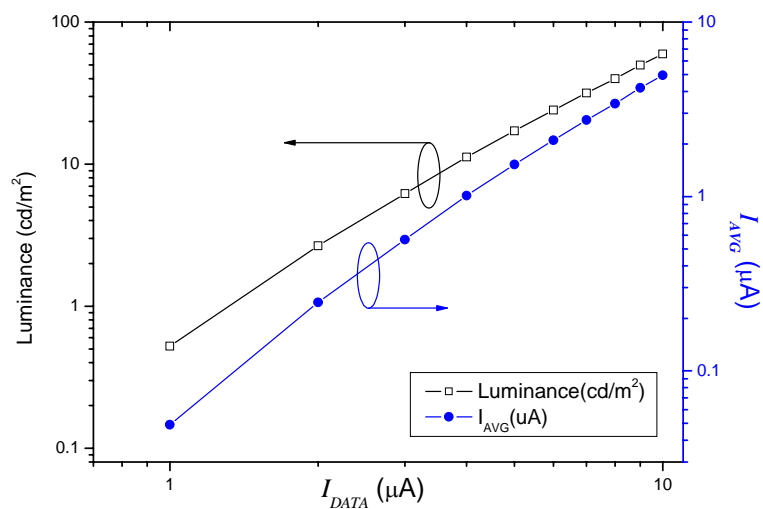


Fig. 4-10  $I_{AVG}$  and luminance versus  $I_{DATA}$ .

### 4.4.3 Display Image

In the following, we display an image on AMOLED. Fig. 4-11(a) is the desired image and Fig. 4-11(b) is the displayed one. The dark dots are due to the TFTs damaged resulting from ESD during fabrication processes. As dim columns/rows are concerned, the non-uniformity of input voltage/current can be improved by the fabrication of circuit system. For example, the resistance can be replaced by accurate resistance. At the same time, the crosstalk can be improved by enhancing the purification of substrate.

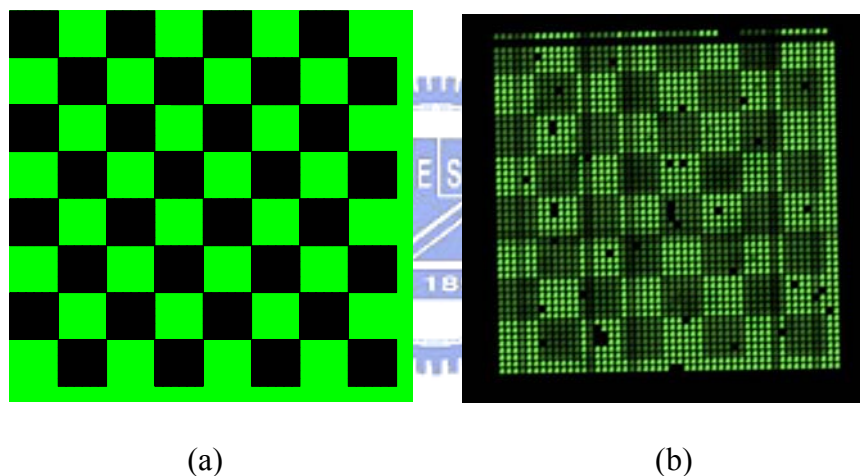


Fig. 4-11 (a) The image we plan to display and (b) the real image on panel.

Table 4-4 lists the specifications of the prototyped AMOLED panel. The panel is a bottom-emission type, and its pixels have an aperture ratio of 52 %. The driving signals are provided by external driving circuit system. Moreover, the luminance ( $200 \text{ cd/m}^2$ ) of the panel is suited to portable devices. The frame rate of the image in Fig. 4-9 is 60 Hz and displays 8 gray scales. The advanced gray levels should be controlled by IC.

Table 4-4. The specifications of AMOLED panel.

<b>Specifications</b>		
Panel size	mm <sup>2</sup>	100 × 100
Display area size	inch	0.7-inch ( 12.5 mm × 12.5 mm )
Pixel size	Um <sup>2</sup>	250 × 250
Aperture ratio	%	52
Pixel number	-	50 × 50
Driving method	-	Current driving scheme
Pixel circuit	-	4TFT + 2Cap
Data driver	-	Constant current source circuit
Scan driver	-	Switching array circuit
Emission type	-	Bottom emission
Color	-	Mono color
Frame frequency	Hz	60 Hz
Max. luminance	cd/m <sup>2</sup>	200
Non-uniformity	%	< 15
Gray level	-	8 gray scales

#### 4.5 Summary

In comparison,  $I_{AVG}$  of the adaptive current scaling pixel circuit achieves the widest range of driving current, compared to current-driven and current-mirror pixel circuits. Hence, at the same programming data current, the lowest gray levels are displayed by the adaptive current scaling pixel circuit. In other words, the adaptive current scaling pixel circuit can be driven by a larger  $I_{DATA}$  to shorten the programming time. Moreover, the adaptive current scaling pixel circuit also has the compensation function for the process- and aging-induced threshold voltage variation so that the uniform images can be achieved. The non-uniformity is about 14.4 % without concerning dark dots, as shown in Fig. 4-8. Such an AMOLED can display 8 gray scales and the results have achieved with the characteristics of adaptive current scaling pixel circuit.

# Chapter 5

## *Conclusion and Future Work*

---

### 5.1 Conclusion

We have designed and fabricated the AMOLED panel with adaptive current scaling pixel circuits according to the characteristic of adaptive current scaling pixel circuit. The OLED devices are deposited on the active area with  $50 \times 50$  pixel array. Moreover, the driving circuits include operational amplifier circuit, constant current source circuit and switching array circuit are designed and fabricated. For the integration of system, the driving signals are generated by FPGA and are transferred to suitable voltage/current level values for adaptive current scaling pixel circuit by passing through the driving circuit system. As result, the AMOLED panel is turned on successfully. Dark dots and dim columns/rows can be improved by the fabrication of substrate and circuit system. The AMOLED panel can display 8 gray scales and the results have achieved with the characteristics of adaptive current scaling pixel circuit.

By comparing the adaptive current scaling pixel circuit with conventional current driven pixel circuit and current mirror pixel circuit, the adaptive current scaling pixel circuit can effectively compensate the threshold voltage variation and improve the charging time. When a low  $I_{DATA}$  is used to express a low gray scale, the conventional current driven pixel circuit has a problem of programming time delay without current scaling function. On the contrary, when a high  $I_{DATA}$  is used to express a high gray scale, the current mirror circuit has a problem of high power

consumption due to a fixed current scaling ratio. The adaptive current scaling pixel circuit has non-linear current scaling function that has a high scaling ratio at low current levels and a low scaling ratio at high current levels. When  $I_{DATA}$  varies from 0.2 to 10  $\mu\text{A}$ , the adaptive current scaling pixel circuit can provide  $I_{AVG}$  ranging from 3 nA to 5  $\mu\text{A}$ . The wider range of  $I_{AVG}$  levels can be achieved by this circuit in comparison with the conventional current driven pixel circuit (0.2 to 10  $\mu\text{A}$ ) and the current mirror pixel circuit (0.01 to 2  $\mu\text{A}$ ). At the same programming data current, the lowest gray levels are displayed by the adaptive current scaling pixel circuit. Therefore, using adaptive current scaling pixel circuit, we expect to minimize the programming time at low current levels, which are supposed to be ideal characteristics for a large size and high resolution AMOLED based on a-Si:H TFTs.



## 5.2 Future Work

The AMOLED is recommended to use different R, G, and B OLED materials to develop full color. Moreover, the varieties of gray scales can be controlled by applying proper data driver IC.

An AMOLED display can be formed by combining adaptive current scaling pixel circuit with OLED. This concept can be also applied to display array's current-driven scheme, such as large size LED display array and backlight.

Besides, the digital signals are transferred to controlling signals for panel by the external driving circuits and the testing fixture. The module consists of driving circuits and testing fixture can be regarded as a testing platform for LED and OLED arrays. Therefore, these arrays can be designed according to the probes amounts and dimensions in the testing fixture and turned on by external driving circuit system.

After that, the characteristics can be measured. The driving circuit system can be, therefore, widely used for advanced research.

OLED has many advantages, such as fast speed, good color, excellent viewing angle and high contrast ratio. Although OLED displays have tremendous potential, there are some challenges must be overcome before reach full potential. The first is lifetime. A display must last a minimum of 10,000 hours [23]. The second is size. Larger OLED panels are needed to compete with LCD. The third is low price. If these challenges are overcome, OLED might be an ideal display in the future.



# Reference

---

- [1] C.W. Tang and S. Van Slyke, "Organic Electroluminescent Diodes," Appl. Phys. Lett., Vol. 51, pp. 913, 1987.
- [2] G. Gu and S.R. Forrest, "Design of Flat-Panel Displays Based on Organic Light Emitting Devices," IEEE J. Sel. Topics Qun. Electronics, Vol. 4, pp. 83, 1998.
- [3] T. Tohma, "Recent progress in Development of Organic Electroluminescent Display Devices," in Int. Display Research conference (IDRC) Dig. Tech. Papers, 1997, F1.1.
- [4] Y. Kijima, N. Asai, N. Kishii, and Tamura, "RGB Luminescence from Passive-Matrix Organic LED's," IEEE Trans. Electron Devices, Vol. 44, pp.1222, Aug. 1997.
- [5] E. I. Haskal, M. Buechel, J. F. Dijksman, P. C. Duineveld, E. A. Meulenlamp, C. A. H. A. Mutsaers, A. Sempel, P. Snijder, S. I. E. Vulto, P. van de Weijer, S. H. P. M. de Winter, "Ink Jet Printing of Passive-Matrix Polymer Light Emitting Displays," SID 2002, pp. 776, 2002.
- [6] J. J. Lih, C. F. Sung, C. H. Li, T. H. Hsiao and H. H. Lee, "Comparison of a-Si and Poly-Si for AMOLEDs," SID 04 DIGEST, pp.1504, 2003.
- [7] Z. Meng, H. S. Kwok and M. Wong, "Metal-Induced Unilaterally Crystallized Polycrystalline Silicon Thin-Film Transistor Technology for Active-Matrix Organic Light-Emitting Diode Displays with Reduced Susceptibility to Cross-Talk," SID 02 Digest, pp.976, 2002.
- [8] J.H. Kim and J. Kanicki, "200 dpi 3-a-Si:H TFTs Voltage-Driven AM-PLEDs,"



SID 03 Digest, pp.18, 2003.

- [9] T. Sasaoka, M. Sekiya, A. Yumoto, J. Yamada, T. Hirano, Y. Iwase, T. Yamada, T. Ishibashi, T. Mori, M. Asano, S. Tamura and T. Urabe, "A 13.0-inch AM-OLED Display with Top Emitting Structure and Adaptive Current Mode Programmed Pixel Circuit (TAC)," SID 01 DIGEST, pp.384-386, 2001.
- [10] Y. He, R. Hattori, and J. Kanicki, "Current-Source a-Si:H Thin-Film Transistor Circuit for Active-Matrix Organic Light-Emitting Displays," in IEEE Electron Device Lett., vol. 21, no. 12, pp. 590-592, 2000.
- [11] Y. He, R. Hattori, and J. Kanicki, "Improved A-Si:H TFT pixel electrode circuits for active-matrix organic light emitting displays," in IEEE Trans. Electron Devices, vol. 48, no. 7, Jul, pp. 1322-1325, 2001.
- [12] J. kanicki, J. H. Kim, J. Y. Nahm, Y. He, and R. Hattori, "Amorphous Silicon Thin Film Transistors Based Active Matrix Organic Light Emitting Display," IDW 01, pp.315-318, 2001.
- [13] Y. Hong, J. Y. Nahm and J. Kanicki, "200 dpi 4-a-Si TFTs Current-Driven AM-PLEDs," SID 03 Digest, pp.22-25, 2003.
- [14] A. Nathan, S. Alexander, K. Sakariya, P. Servati, S. Tao, D. Striakhilev, A. Kumar ,S. Sambandan, S. Jafarabadiashtiani, Y. Vigranenko ,C. Church, J. Wzorek, P. Arsenault "Extreme AMOLED Backplanes in a-Si with Proven Stability ," SID 04 Digest, pp.1508-1511, 2003.
- [15] J. H. Lee, B. H. You, W. J. Nam, H. J. Lee and M. K. Han, "A New a-Si TFT Pixel Design Compensating Threshold Voltage Degradation of TFT and OLED," SID 04 Digest, pp.264-267, 2003.

- [16] J. C. Goh, C. K. Kim and Jin Jang, "A New Pixel Design for Amorphous-Silicon Backplane of Active Matrix Organic Light-Emitting Diode Displays," SID 04 Digest, pp.276-279, 2004.
- [17] Y. C. Lin, H. P. D. Shieh, C. C. Su, H. Lee, and J. Kanicki, "A Novel Current-Scaling a-Si:H TFTs Pixel Electrode Circuit for Active Matrix Organic Light-Emitting Displays," SID 05 Digest, pp. 846-848, 2005.
- [18] A. Yumoto, M. Asano, H. Hasegawa, and M. Sekiya, "Pixel-driving methods for large-sized poly-Si AM-OLED displays," in Proc. Int. Display Workshop, 2001, pp. 1395-1398, 2001.
- [19] J. Lee, W. Nam, S. Jung, and M. Han, "A New Current Scaling Pixel Circuit for AMOLED," in IEEE Electron Device Lett., vol. 25, no. 5, May 2004, pp. 280-282, 2004.
- [20] Y. C. Lin, H. P. D. Shieh, and J. Kanicki, "A Novel Current-Scaling a-Si:H TFTs Pixel Electrode Circuit for Active-Matrix Organic Light-Emitting Displays," in IEEE Elec. Dev. Trans., vol. 52, pp. 1123-1131, 2005.
- [21] H Lee, J. Kanicki, Y. C. Lin and H. P. D. Shieh, "Current-Scaling a-Si:H TFT Pixel Electrode Circuit for AM-OLEDs," SID 06 Digest, pp. 1968-1971, 2006.
- [22] Phil Downen, "A Closer Look at Flat-Panel-Display Measurement Standards and Trends," Information Display, pp.16~21, Jan. 2006.
- [23] Shoichi Iino and Satoru Miyashita, "Printable OLEDs Promise for Future TV Market," SID 06 Digest, pp. 1463-1466, 2006.